Title

Liquefaction and Cyclic Softening at Balboa Boulevard during the 1994 Northridge Earthquake

Journal

Journal of Geotechnical and Geoenvironmental Engineering, 147(2)

ISSN

1090-0241

Authors

Pretell, Renmin
Ziotopoulou, Katerina
Davis, Craig A

Publication Date

2021-02-01

DOI

10.1061/(asce)gt.1943-5606.0002417

Peer reviewed

Case Study

Liquefaction and Cyclic Softening at Balboa Boulevard during the 1994 Northridge Earthquake

Renmin Pretell, S.M.ASCE[1]; Katerina Ziotopoulou, A.M.ASCE[2]; and Craig A. Davis, M.ASCE[3]

Abstract: The seismic performance of Balboa Boulevard during the 1994 M_W 6.7 Northridge earthquake was examined through nonlinear deformation analyses (NDAs) using advanced tools to (1) investigate the failure mechanism leading to ground deformations at this site; (2) evaluate the accuracy of the adopted analysis methods, engineering procedures, and state-of-the-art tools to reasonably estimate horizontal ground displacements; and (3) identify key factors and parameters contributing to earthquake-induced ground deformations at this site. One-dimensional (1D) liquefaction vulnerability indexes (LVIs) and permanent displacements using Newmark sliding block analyses were also estimated and compared against ground deformations observed after the earthquake. The geotechnical characterization of Balboa Boulevard was assessed based on field and laboratory data obtained from two investigation campaigns. Transitional probability geostatistics were used to develop stratigraphic models that capture the heterogeneity and the spatial variability patterns of sand-like and clay-like soils present at this site. The stratigraphic models were implemented in the finite difference software FLAC and the behavior of sand-like and clay-like soils simulated using the PM4Sand and PM4Silt constitutive models, respectively. Sensitivity analyses were performed to address uncertainties associated with the spatial variability of soils, input ground motions, the proportion of sand-like and clay-like soils within the soil deposit, and the strength properties of these materials. Results from NDAs suggest that a compounded effect of both liquefaction of sand-like soils and cyclic softening of clay-like soils led to the excessive ground deformations at Balboa Boulevard. This study sheds light on the importance of using appropriate engineering procedures and numerical modeling protocols in the prediction of deformation patterns, the selection of key input parameters, as well as the applicability of LVIs in complex sites. **DOI: 10.1061/(ASCE)GT.1943-5606.0002417.**

Author keywords: Liquefaction; Cyclic softening; Case history; Nonlinear deformation analyses; Spatial variability; Ground deformation.

Introduction

Nonlinear deformation analyses (NDAs) are a valuable tool for assessing the seismic performance of geosystems subject to the effects of strength loss and the associated deformations caused by shaking. NDAs provide an improved basis for estimating deformations over simplified methods that do not account for the dynamics of the system or are limited to idealized geometries or conditions. The capability of NDAs to reproduce deformation patterns and failure mechanisms allows for the identification of critical parameters and factors leading to ground displacements and the associated engineering demands they impose on infrastructure, which in turn improves engineering judgment and informs decision-making.

Case histories have always been a valuable source of information to improve the understanding of failure mechanisms and propel advancements in engineering procedures. Over the past decade, case histories have been the topic of NDAs to evaluate the applicability of numerical analysis procedures and the tools these employ (e.g., Bray and Luque 2017; Luque and Bray 2017; Montgomery et al. 2017; Kiernan and Montgomery 2018; Boulanger et al. 2019; Boulanger 2019; Chaloulos et al. 2019; Tasiopoulou et al. 2019; Luque and Bray 2020). Simplified procedures such as liquefaction vulnerability indexes (LVIs) and Newmark sliding block analyses have offered an alternative approach to evaluating the seismic performance of geosystems at a preliminary level as they carry inherent assumptions and require conditions with limited applicability (Boulanger et al. 2019).

The performance of Balboa Boulevard during the 1994 M_W 6.7 Northridge earthquake is a well-documented case history of earthquake-induced ground deformations and their effect on buried infrastructure. Damages observed at Balboa Boulevard after the earthquake include the formation of extensional and compressional failure zones and an overall horizontal displacement of 50 cm (Holzer et al. 1996, 1999). The failure mechanism behind these observations has been previously assessed by several authors, but it was still not fully understood. The availability of subsurface data, ground displacement measurements, and ground motion recordings makes the Balboa Boulevard case history well suited for (1) the numerical investigation of the failure mechanism leading to ground deformations at this site; (2) the evaluation of the accuracy of the adopted analysis methods and engineering procedures to reasonably capture the observations; and (3) the identification of key factors leading to ground deformations at this site.

For this paper, the seismic performance of Balboa Boulevard during the Northridge earthquake was examined through NDAs using state-of-the-art numerical tools with the following objectives:

[1]Graduate Student Researcher, Dept. of Civil and Environmental Engineering, Univ. of California, Davis, CA 95616 (corresponding author). ORCID: https://orcid.org/0000-0001-8552-2905. Email: rpretell@ucdavis.edu

[2]Assistant Professor, Dept. of Civil and Environmental Engineering, Univ. of California, Davis, CA 95616. ORCID: https://orcid.org/0000-0001-5494-497X

[3]Consultant, Craig A. Davis Engineering, 27017 Vista Encantada Dr., Santa Clarita, CA 91354.

Note. This manuscript was submitted on March 17, 2020; approved on July 30, 2020; published online on December 10, 2020. Discussion period open until May 10, 2021; separate discussions must be submitted for individual papers. This paper is part of the ***Journal of Geotechnical and Geoenvironmental Engineering***, © ASCE, ISSN 1090-0241.

(1) to investigate the failure mechanism leading to ground deformations at Balboa Boulevard; (2) to evaluate the accuracy of the adopted analysis methods, engineering procedures, and state-of-the-art tools, to reasonably estimate horizontal ground displacements; and (3) to identify key factors and parameters contributing to earthquake-induced ground deformations at this site. Subsurface conditions at Balboa Boulevard were evaluated based on the understanding of the geologic setting of the region as well as field and laboratory data from investigation campaigns carried out along two parallel alleys. Two-dimensional NDAs were performed using stochastic realizations, developed based on a transition probability approach, for the interbedded portions of the stratigraphy. The sand-like and clay-like portions were modeled using the PM4Sand (Boulanger and Ziotopoulou 2017) and PM4Silt (Boulanger and Ziotopoulou 2018, 2019) constitutive models, respectively. Uncertainties associated with the selection of input parameters were accounted for by using various equally possible stratigraphic and ground motion realizations, as well as different I_c cutoff values differentiating sand-like from clay-like soils, cyclic strengths assigned to sand-like soils, and undrained shear strengths assigned to clay-like soils, water table depths, shear wave velocity values, ground surface gradients, and other input parameters and modeling choices. A total of 302 NDAs were performed. Simplified methods to assess liquefaction damage (LVIs) and Newmark sliding block analyses were also used to evaluate the accuracy of these methods to predict earthquake-induced ground surface damage. The results obtained with these various analysis methods suggested liquefaction of sand-like soils together with cyclic softening and shear failure of clay-like soils as the failure mechanism leading to ground deformations at Balboa Boulevard and demonstrated limitations of the simplified methods. Furthermore, results from the examination of this case history are expected to provide insight into critical factors leading to ground deformations and thus improve field and laboratory investigations, the selection of parameters for forward predictions via numerical simulations, and the use of finite difference solutions combined with transitional probability geostatistics and advanced constitutive models.

Ground Failure at Balboa Boulevard during the Northridge Earthquake

The Northridge earthquake was a M_W 6.7 crustal event that occurred on January 17, 1994, at 4:31 a.m. near Northridge, California, in the San Fernando Valley [Figs. 1(a and b)]. At the time, the Northridge earthquake was regarded as the costliest natural disaster in US history and the largest earthquake in the Los Angeles area after the 1971 San Fernando earthquake (Holzer et al. 1999). It caused significant damage to residential and commercial structures, the disruption of utilities and lifelines, landslides, and the failure of soil embankments (e.g., Hecker et al. 1995b; Stewart et al. 1996).

Balboa Boulevard is a north–south-oriented street located on the northern side of the San Fernando Valley [Fig. 1(c)] in a 1.6%–3.6% sloping area previously mapped as nonliquefiable due to the overall relatively deep groundwater table in the area (Stewart et al. 1994). A peak ground acceleration (PGA) of $0.84g$ was recorded at the closest free field station [Rinaldi Receiving Station (RRS)] in the 228° component. Ground deformation at Balboa Boulevard caused the breakage of two water trunk lines, one gas transmission pipeline (Old Line 120), and one gas distribution pipeline (O'Rourke and Palmer 1994; Holzer et al. 1996), the subsequent formation of ground craters, and the ignition of fire [Fig. 2(a)]. Zones of extension [Fig. 2(b)] and compression [e.g., Fig. 2(c)] were observed after the earthquake, about 300 m apart in the north–south direction, within a larger damaged area spanning roughly 600 m in length and width (Stewart et al. 1996). Fig. 2(d) is a plan view of the damage mapped around the Balboa Boulevard area pertinent to this study, including the approximate location of extensional and compressional ground deformations [based on Hecker et al. (1995b)]. Cracks and displacements had an overall south-southeast orientation, as indicated by the arrows. No typical evidence of liquefaction such as sand boils was found.

Several authors have reported magnitudes of the visible ground deformation patterns in the area surrounding Balboa Boulevard.

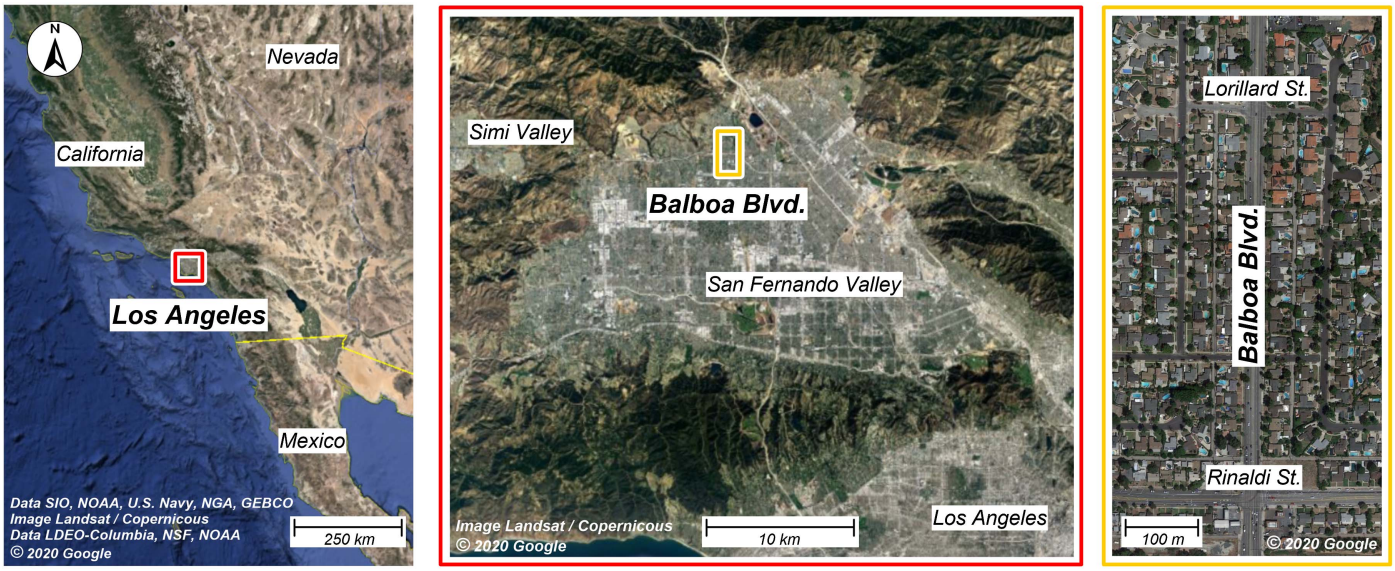

Fig. 1. Location of the Balboa Boulevard site; (a) Los Angeles area (map data © 2020 Google, Data SIO, NOAA, U.S. Navy, NGA, GEBCO, Image Landsat/Copernicious, Data LDEO-Columbia, NSF, NOAA); (b) San Fernando Valley (map data © 2020 Google, Image Landsat/Copernicous); and (c) Balboa Boulevard (map data © 2020 Google).

J. Geotech. Geoenviron. Eng., 2021, 147(2): 05020014

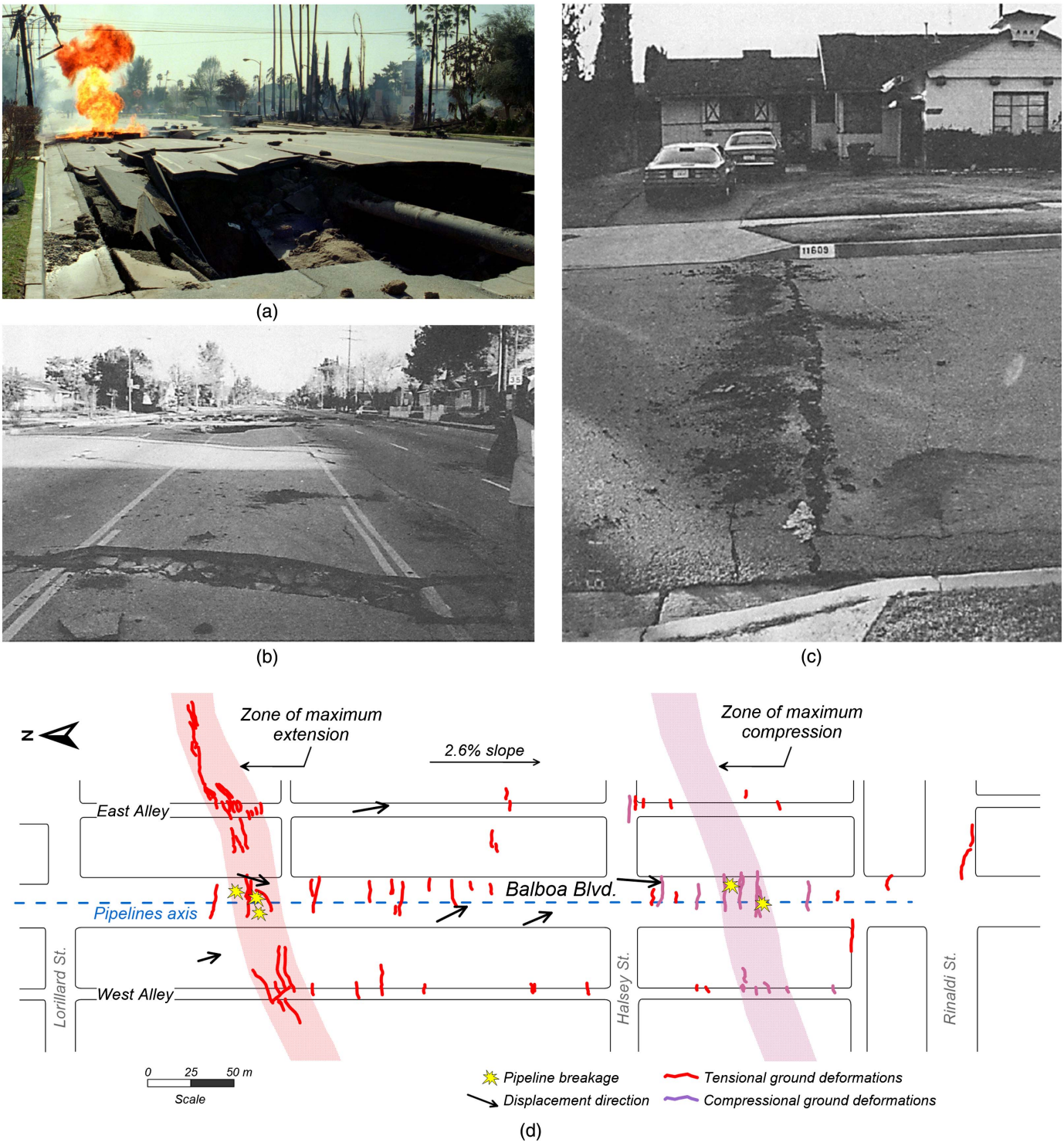

Fig. 2. Observed damage at Balboa Boulevard after the 1994 Northridge earthquake: (a) ground craters and fire (Copyright © 1994, Los Angeles Times, used with permission); (b) extensional failure across Balboa Boulevard [reprinted with permission from J. P. Stewart, R. B. Seed, J. D. Bray, "Incidents of ground failure from the 1994 Northridge earthquake", *Bulletin of the Seismological Society of America*, 86(1B), pp. S300–S318, 1996, DOI, © Seismological Society of America]; (c) compressional failure across Ostrom Street, a parallel alley 380 m west of Balboa Boulevard [reprinted with permission from J. P. Stewart, R. B. Seed, J. D. Bray, "Incidents of ground failure from the 1994 Northridge earthquake", *Bulletin of the Seismological Society of America*, 86(1B), pp. S300–S318, 1996, DOI, © Seismological Society of America]; and (d) plan view of observed ground damage distinguishing between extensional and compressional deformations (adapted from O'Rourke and Palmer 1994).

The Los Angeles Bureau of Engineering (LABE 1995) estimated displacements of 45 cm in the extensional zone through ground surveying along the streets. Holzer et al. (1996, 1999) determined overall displacements of 50 cm at both the extensional and compressional zones based on street centerline surveys. Hecker et al. (1995a) found approximate displacements of 33–54 cm in extension, and 27–42 cm in compression, based on the measurement of cumulative crack openings. Aerial photographs indicated

values ranging from 48 to 90 cm. Recognizing that zones of compressional deformations are more challenging to measure than extensional ones, and the fact that aerial photographs at that time had a lower resolution with unquantifiable errors associated to the measurements, herein a reference lateral displacement of 50 cm was considered for the overall site in this study. Hecker et al. (1995b) indicated that vertical displacements after the earthquake were generally small (a few centimeters) with localized vertical offsets along cracks up to about 25 cm (Stewart et al. 1996). Vertical displacements tended to be downward near the zone of extension and upward near the zone compression (Stewart et al. 1996; SCGC and PG&E 2000), consistent with a sliding mass failure mechanism (Stewart et al. 1996). Findings regarding vertical displacement magnitudes from a leveling survey by the City of Los Angeles were not compatible with curb and gutter surveys (SCGC and PG&E 2000) and thus they are not discussed herein.

Site Conditions

Geologic Setting and Stratigraphy

The San Fernando Valley is a structural valley filled with up to 4,500 m of Tertiary sedimentary rock overlain by alluvial sediments (Wentworth and Yerkes 1971). Soils consist of Holocene alluvial gravels, sands, and finer sediments that were deposited by sediment-laden floodwaters in the valley floor in thicknesses ranging from 8 to 12 m (Holzer et al. 1999). Source rocks for these materials include the fine-grained Cenozoic and Mesozoic rocks from the surrounding mountains. Underlying the alluvial deposits, there is an older unit from the late Pleistocene, denominated Saugus Formation, consisting of slightly indurated fluvial sediments of late- to mid-Pliocene age (Holzer et al. 1999).

Holzer et al. (1999) identified four geologic units at Balboa Boulevard (Fig. 3). Unit A, at the top, is a less than 1-m-thick layer

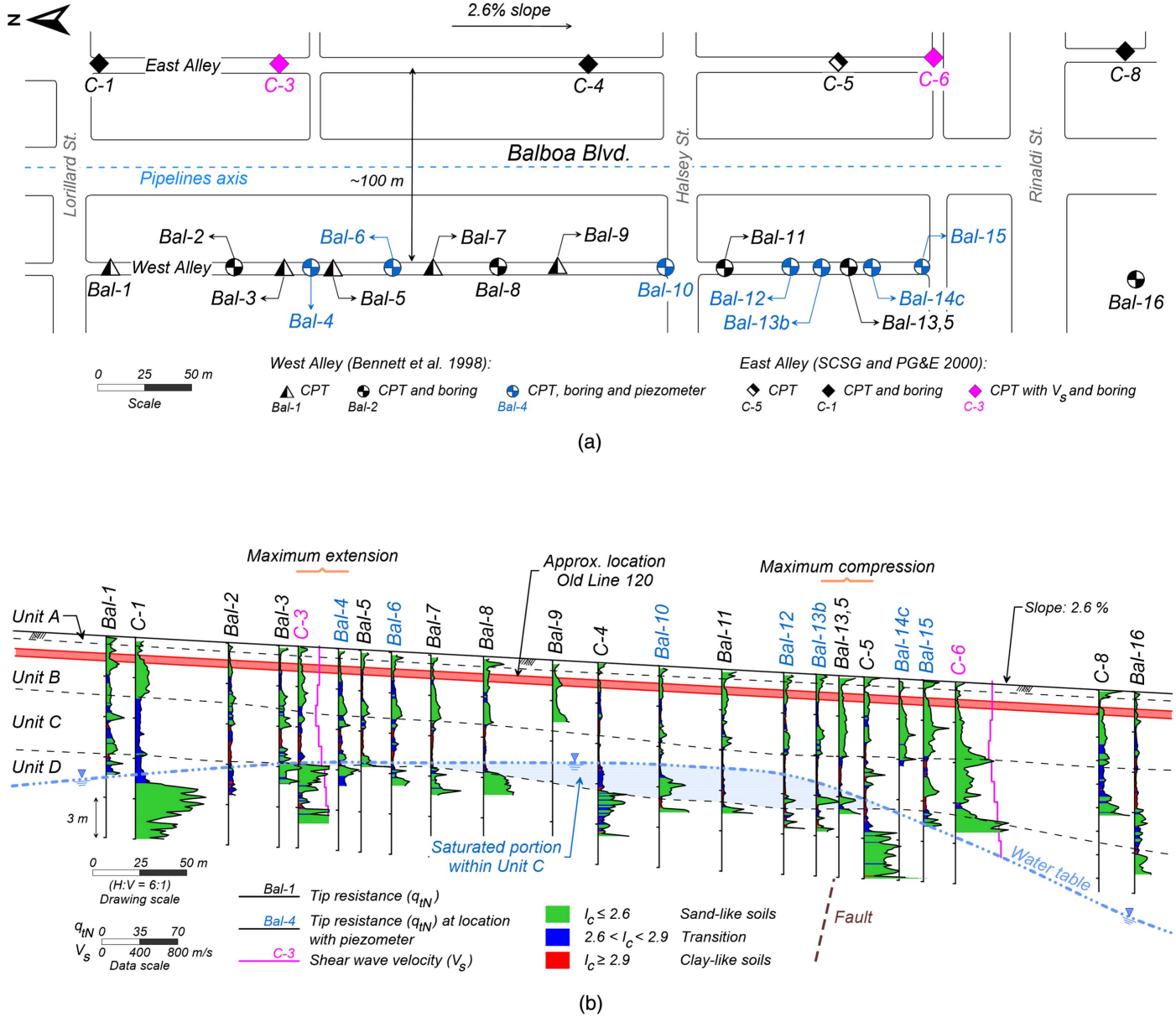

Fig. 3. Field investigations and site information: (a) plan view of the field investigations along the east and west alleys (data from Southern California Gas Company and Pacific Gas Electric Company 2000); (b) cross section of Balboa Boulevard along west alley showing main subsurface features and data (adapted from Holzer et al. 1999, © ASCE).

J. Geotech. Geoenviron. Eng., 2021, 147(2): 05020014

that consists of fill, reworked sandy silt, and lean clay with sand. Unit B is the uppermost portion of the Holocene deposit and consists of sheet flood and debris flow materials; whereas Unit C, the lowermost portion, is a heterogeneous fluvial deposit with a high fines content (FC). Unit C has been identified by various researchers as the critical layer at this site. Finally, Unit D is interpreted to be part of the Saugus Formation. Differentiating these geologic units or facies is critical for both the assignment of geotechnical properties and for the geostatistical analysis of the spatial variability of soils at the Balboa Boulevard site.

Geotechnical Investigations

Two geotechnical investigation campaigns were carried out along parallel alleys located about 50 m west and east of Balboa Boulevard, respectively. The first investigation campaign was led by USGS in April 1995 and consisted of 17 cone penetration tests (CPTs), 13 of which were paired with drilled borings. The drilling program of borings included the collection of samples using Shelby tubes as well as the performance of standard penetration tests (SPTs), field vane tests (FVTs), and the installation of monitoring wells. Soil samples were subsequently tested in the laboratory for index properties. Results from field and laboratory tests along the west alley were described by Bennett et al. (1998), whereas interpretation of these data was carried out by Holzer et al. (1999). The second investigation campaign was led by Woodward-Clyde Consultants (WCC) in October of 1996 by request of the Southern California Gas Company and the Pacific Gas and Electric Company (SCGC and PG&E 2000) (made available for this study by PG&E in coordination with Professor N. A. Abrahamson). A total of six CPTs were performed along the east alley together with five borings that included SPT testing and the collection of soil samples. Additionally, two seismic CPTs were carried out and shear wave velocity (V_s) profiles estimated. Soil samples were tested for index properties. Digital CPT data from the west alley were available on the USGS website, whereas paper-printed CPT data from the east alley were provided and digitalized for purposes of this study. Fig. 3(a) presents a plan view of Balboa Boulevard showing the locations of CPTs, borings, and seismic CPTs performed as part of the two investigation campaigns. Fig. 3(b) shows a north–south cross section along with the most relevant data.

The two field investigation campaigns were performed 1–2 years after the earthquake. The effects of preshaking on cone penetration resistance in sandy soils have been investigated by various researchers based on observations from case histories and results from centrifuge tests. Findings from case histories with CPT records pre and postearthquake (e.g., Boulanger et al. 1995; Holzer and Youd 2007; Chameau et al. 1998) suggested that only mild increases of tip resistance might occur in initially loose soils, if any. Findings from centrifuge tests (e.g., El-Sekelly et al. 2018; Darby et al. 2019) indicated that there is potential for increases of penetration resistances after significant preshaking. The difference between findings from case histories and centrifuge tests could be attributed to a compensating effect between strength gain due to particle rearrangement after liquefaction (i.e., increase of relative density D_R) and the loss of other effects such as aging and cementation, that are typically not reproduced in the laboratory. In addition, particle size effects may play a role in CPT centrifuge measurements that increase for increasing D_R values (Sturm 2019), although that effect would likely be uniform before and after shaking events, and it remains unclear whether any increases in CPT resistance are due to an increase in the D_R or particle size effects per se. Based on these observations and the inherent heterogeneity of subsurface conditions at Balboa Boulevard, the effect of preshaking was expected to be relatively small compared to issues pertaining to the spatial variability of soils. Data from the aforementioned postearthquake investigations were considered representative of the preearthquake conditions for the work presented herein.

Interpretation of Data from Field and Laboratory Investigations

The agreement of data from investigations carried out along the west and east parallel alleys was evaluated, such that both would be used to characterize the subsurface at Balboa Boulevard. The encountered geologic units, boring logs, cone penetration resistances, and laboratory test results including the Universal Soil Classification System (USCS), plasticity index (PI), and FC were examined. In terms of geologic units, Holzer et al. (1999) identified four different ones previously described as Units A–D from top to bottom, based on findings from field investigations along the west alley, while WCC reported three units based on both the west and east alley geotechnical investigations by essentially lumping Units A and B together. Data from both alleys were also in good agreement with the exception of discrepancies encountered at the south end of the east alley [CPTs C-6 and C-8 in Figs. 3(a and b)]. At these locations sandy soils with gravels, fragments of siltstone, and sandstone were located, together with an overall higher tip resistance [Fig. 3(b)]. Data from these locations, including cone penetration resistances, laboratory test results, and V_s measurements (CPT C-6), were considered unrepresentative of the overall study site and disregarded herein.

The Soil Behavior Type (SBT) Index I_c (Robertson and Wride 1998; Zhang et al. 2002) was estimated from CPT tip resistance and sleeve friction, and was used to differentiate between sand-like and clay-like soils. Using an I_c cutoff of 2.6, as commonly considered in practice (Robertson and Wride 1998), the percentage of sand-like soils ($I_c \leq 2.6$) within Units A, B, C, and D were 85%, 70%, 20%, and 55%, respectively. The I_c cutoff value depends on several factors including mineralogy, PI, and the stress history of soils (Robertson and Wride 1998); thus, alternative site-specific I_c cutoffs could also be justified (Boulanger and Idriss 2015). Herein, an applicable I_c was examined for the Balboa Boulevard Unit C, based on CPT investigations paired with borings that had USCS data available. The estimated SBT soil category (sand-like or clay-like) was compared to the corresponding USCS category at a similar depth. Soils with USCS classification of SM (silty sand), SC (clayey sand), and ML (silt) were expected to be categorized as sand-like soils, and CL (lean clay), CL-ML (silty clay), and CH (fat clay) as clay-like soils. The main assumptions of this methodology included (1) both CPT-sheared and sampled soils from borings share the same characteristics; and (2) the data available for this evaluation are representative of Unit C. Fig. 4 shows the data on the Q_{tn}–F_r space (normalized cone resistance versus normalized friction ratio) and various I_c cutoff boundaries separating the space into sand-like and clay-like zones. An $I_c = 2.9$ led to the minimum overall error (defined as the addition of the distances from all the data points to a chosen I_c boundary) and was thus selected as the applicable site-specific I_c cutoff for Balboa Boulevard. The presence of clay-like soils within Unit C was supported by PI values, which ranged from 2 to 31 with a median of 12 and only 14 out of the 81 data points with a PI lower than 7. Given the assumptions behind this evaluation, the I_c cutoff of 2.9 is best considered as a reference upper bound used to define a transitioning zone between sand-like and clay-like soils (Fig. 4). Fig. 3(b) presents the location of CPTs with the variation of tip resistance (q_{tN}) with depth, distinguishing soils categorized as sand-like soils ($I_c \leq 2.6$), clay-like soils ($I_c \geq 2.9$), and transitioning soils ($2.6 < I_c < 2.9$).

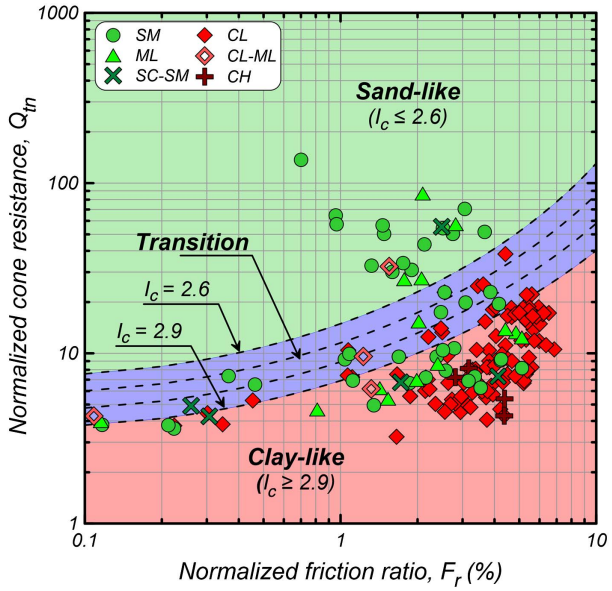

Fig. 4. SBT chart proposed by Robertson (2009) and site-specific data. Selection of applicable I_c cutoff to differentiate sand-like and clay-like soils at Balboa Boulevard.

The proportions of sand-like soils within Unit C associated to I_c cutoffs of 2.7, 2.8, and 2.9 are approximately 30%, 35%, and 55%, respectively. Units A, B, and D were considered to behave predominantly as sand-like soils.

Measured cone penetration resistances were corrected to eliminate biases inherent to the test. Within Unit C, the dimensionless tip resistances q_{tN} ranged from 27 to 134 with a median of 57 for sand-like soils, and from 6.5 to 36 with a median of 15 for clay-like soils. In the remainder of this section, ranges will correspond to the 5th to 95th percentile, preferred over minimum and maximum because they are less sensitive to sporadic peaks or troughs in CPT measurements. The q_{tN} values were corrected due to overburden (q_{t1N}) according to Boulanger and Idriss (2015). Equivalent clean sand corrected tip resistances (q_{t1Ncs}) were estimated by adding an equivalent clean sand adjustment (Δq_{t1N}) as a function of FC of samples from corresponding paired borings and depths to q_{t1N} values. At locations where FC values were not available, the expression proposed by Boulanger and Idriss (2015) to estimate FC as a function of I_c and a fitting parameter C_{FC} was used. The coefficient C_{FC} was calibrated such that median laboratory FC for each unit at every CPT location (i.e., 40%–66% for Unit B, 50%–70% for Unit C, and 20%–60% for Unit D) was approximately matched by the FC estimates. Values for C_{FC} were estimated as 0.05, −0.39, and 0.08 for Units B, C, and D, respectively. A default $C_{FC} = 0$ was used for Unit A due to the sparse data available for this unit. Within Unit C, q_{t1Ncs} ranged from 60 to 140 with a median of 90 for sand-like soils, and from 60 to 90 with a median of 70 for clay-like soils. Correction due to unequal end area was not applied to tip resistances due to the lack of pore pressure data along the west alley, while along the east alley patterns of measurements indicated inadequate saturation of the porous stones (J. T. DeJong, personal communication, 2018). The effect of not applying this correction would be negligible in sand-like soils because pore water pressure would have been near hydrostatic conditions, but in clay-like soils it could lead to a 10%–30% underestimation of measured tip resistances (Robertson 2013).

The relative density (D_R) of sand-like soils was estimated as a function of q_{t1Ncs} and the coefficient C_{dq} (Idriss and Boulanger 2008). The value of C_{dq} ranges from 0.64 to 1.7, with 0.9 being an overall appropriate value (Idriss and Boulanger 2003). By using $C_{dq} = 0.9$ for Unit A, $D_R = 30\%$ was estimated; for Unit B, D_R ranged from 36% to 56% with a median of 46%; for Unit C, D_R ranged from 33% to 71% with a median of 50%; and for Unit D it ranged from 39% to 82% with a median of 52%. Fig. 5 illustrates the methodology for estimating the representative D_R for Unit C and shows how a median value of $q_{t1Ncs} = 90$ was considered representative of sand-like soils within Unit C, thus resulting in the median $D_R = 50\%$. The q_{t1Ncs} of sand-like soils is relatively consistent across the site as inferred by the relatively narrow range of the cumulative distribution [Fig. 5(d)].

The undrained shear strength (s_u) of clay-like soils was estimated from q_t using the bearing capacity equation (Lunne et al. 1985; Kulhawy and Mayne 1990), which depends on the empirical cone factor N_{kt}. The latter ranges from 5 to 20 or higher values [e.g., discussion by Whittle et al. (1989)]. Herein, N_{kt} was estimated as 16.5 based on calibrations against remolded undrained shear strengths from FVTs paired with CPTs. FVTs were performed at the relatively fast shearing rate of 90°/min; thus, s_u values from these tests are considered representative of the undrained cyclic strength of clays under earthquake loading rates (Holzer et al. 1999). The calibration of N_{kt} to determine s_u from q_t measurements was expected to compensate for any underestimation of tip resistance due to the omission of the unequal area correction. Fig. 6 illustrates the methodology for estimating the representative s_u for the clay-like soils of Unit C and shows s_u values of clay-like soils ranging from 34 to 210 kPa, with a median of about 80 kPa. Despite 80 kPa being the median, Fig. 6(d) shows a noticeably wide distribution with $s_u = 50$ kPa being consistent at similar depths among four CPTs located together [Bal-10, Bal-11, Bal-12, and Bal-13b shown in Fig. 3(b)], and equivalent to about the 20th percentile of all data. In addition to s_u, the overconsolidation ratio (OCR) of clay-like soils was estimated using the Stress History and Normalized Soil Engineering Properties (SHANSEP) approach (Ladd and Foott 1974; Ladd 1991). OCRs of clay-like soils within Unit C varied from 1.5 to 15 assuming a typical $s_{u,NC}/\sigma'_{vo}$ of 0.22 (Mesri 1975). These OCRs are consistent with the geologic setting of Balboa Boulevard, i.e., cycles of flooding, deposition, and desiccation (Mitchell and Soga 2005).

Additional engineering parameters were directly obtained from field and laboratory tests or estimated using published correlations. Shear wave velocities (V_s) for Units A, B, C, and D were taken as 220, 200, 240, and 320 m/s, respectively, based on a single V_s profile measured at C-3 [Fig. 3(b)]. Samples from all units were tested for dry and bulk density. Results from these tests, supported by common values from the literature, were used to estimate approximate values for dry and saturated densities and porosity. Given the relatively low degree of precision at which these parameters can be measured and the narrow range of possible values, a dry density of 1,510 kg/m^3, saturated density of 1,890 kg/m^3, and porosity of 0.40 were assigned to all units. Peak friction angles estimated using the correlation by Kulhawy and Mayne (1990) for Units A, B, and D were 32°, 36°, and 36°, respectively. Sand-like and clay-like soils within Unit C had estimated friction angles of 36° and 29.5°, respectively. Permeability values, estimated as a function of I_c (Robertson 2010), for Units A, B, and D were approximately 10^{-5}, 10^{-7}, and 10^{-9} m/s, whereas 10^{-7} and 10^{-9} m/s were estimated for sand-like and clay-like soils within Unit C, respectively.

Groundwater Table

The location of the groundwater table played a key role in this case history. The Balboa Boulevard area had been previously mapped as nonliquefiable by Los Angeles County (1990) given the deep

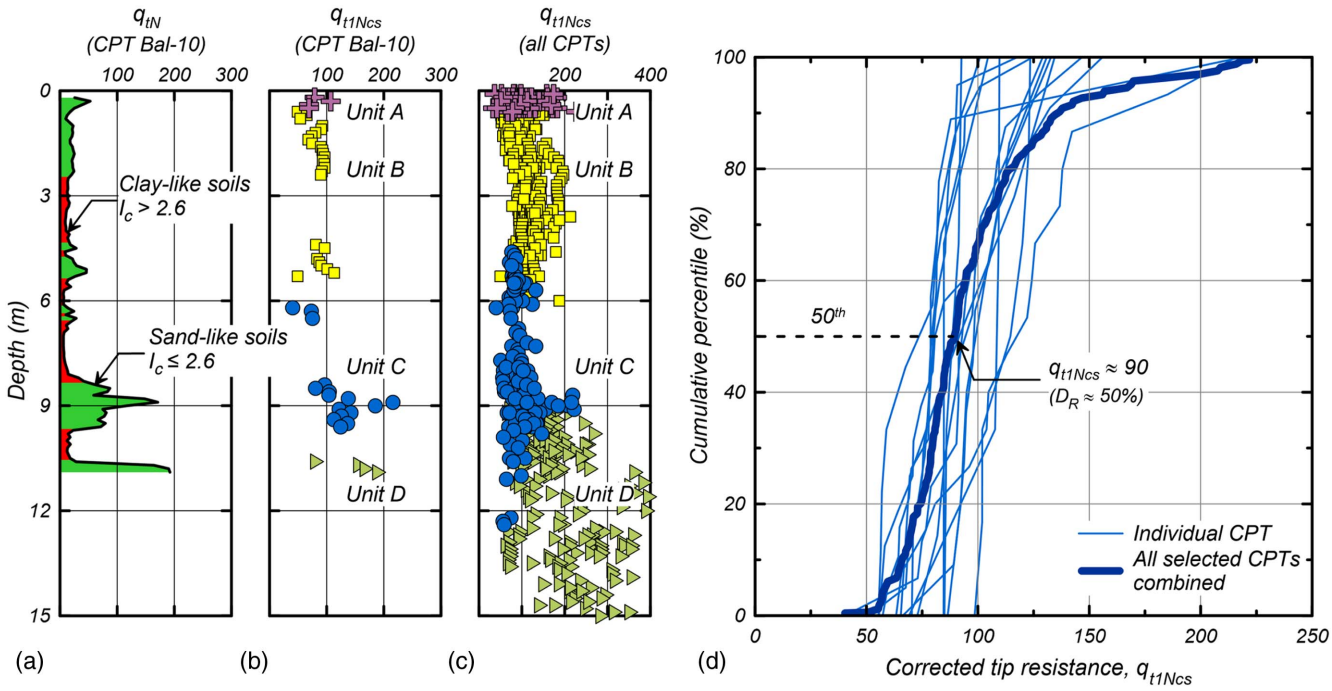

Fig. 5. Cone penetration resistance of sand-like soils from selected CPTs: (a) variation of q_{tN} and SBT with depth at CPT Bal-10; (b) variation of q_{t1Ncs} at CPT Bal-10; (c) variation of q_{t1Ncs} at all CPTs; and (d) cumulative distribution of q_{t1Ncs} within Unit C for all individual CPTs (thin lines), and cumulative distribution of all CPTs combined (thick line).

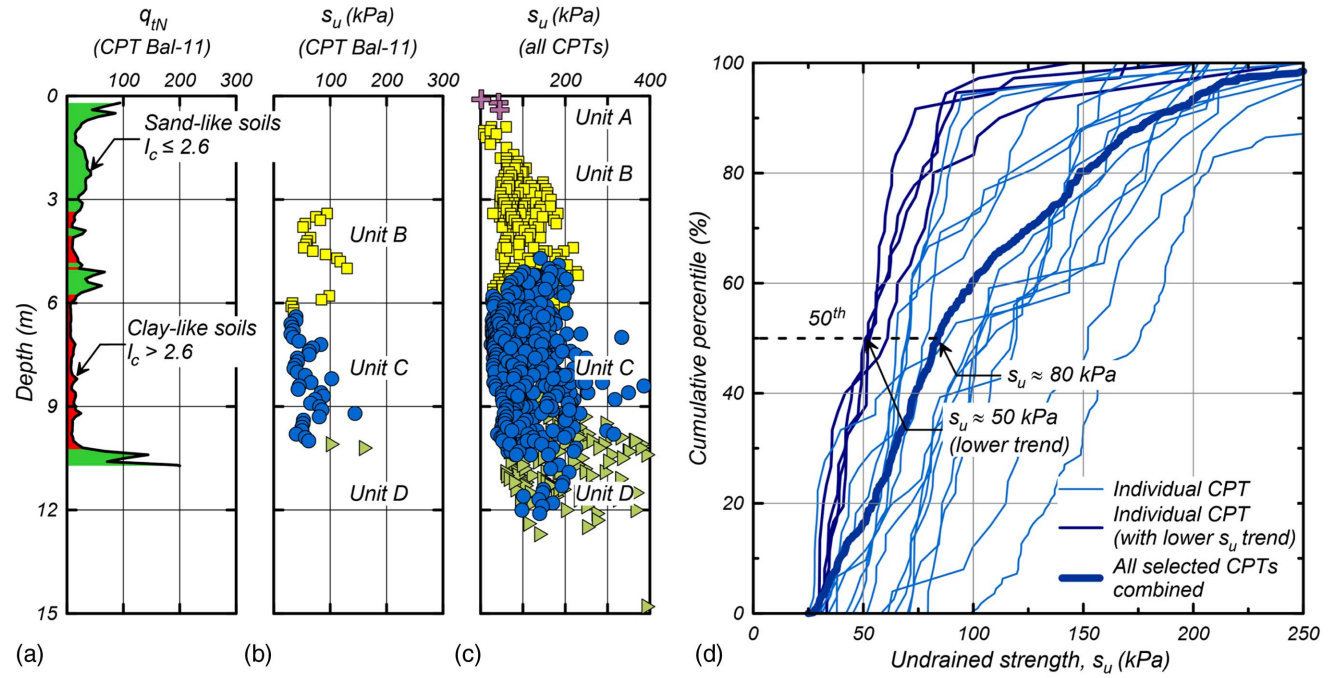

Fig. 6. Undrained shear strength of clay-like soils ($N_{kt} = 16.5$) from selected CPTs: (a) variation of q_{tN} and SBT with depth at CPT Bal-11; (b) variation of s_u at CPT Bal-11; (c) variation of s_u at all CPTs; and (d) cumulative distribution of s_u within Unit C for all individual CPTs (thin lines) and cumulative distribution of all CPTs combined (thick line), with a lower trend of s_u observed at CPTs Bal-10, Bal-11, Bal-12, and Bal-13b.

groundwater table expected at the site based on microzonation studies (Stewart et al. 1994). The groundwater table was located during the geotechnical investigation campaign along the west alley and estimated at depths ranging from 7 to 11 m, consistent with the observations in exploratory borings along the east alley, about a year and a half later. The groundwater table at Balboa Boulevard estimated by Holzer et al. (1999) is illustrated in Fig. 3(b).

The potential for water recharge from the pipelines that broke during the earthquake led to questioning the representativeness of the groundwater table of pre-earthquake conditions, as well as its

J. Geotech. Geoenviron. Eng., 2021, 147(2): 05020014

variable depth encountered during field investigations. Holzer et al. (1999) examined these features based on piezometer monitoring. A total of seven piezometers were installed along the west alley [Fig. 3(b)] and water levels were monitored from July 1995 to December 1996. Based on these readings, the groundwater table was considered stable in time and thus representative of pre-earthquake conditions (Holzer et al. 1999). The stability of the groundwater table was consistent with the darker color of saturated sediments observed during drilling works, which were indicative of long-term hydraulic conditions (Holzer et al. 1999). Potential explanations for the stability of such an uncommon groundwater table shape include a compounded effect of local recharging and seasonal water fluctuations (typically consisting of at least several feet in the upland settings of California) and the presence of perched water (T. L. Holzer, personal communication, 2019). The shape of the groundwater table has also been attributed to the presence of a splay of the Mission Hills fault [Fig. 3(b)] that could be acting as a hydraulic barrier. This fault is consistent with hydrogeologic and stratigraphic observations (Holzer et al. 1999), the tectonic environment, and the site location within the deformation belt along the south flank of the Santa Susana Mountains (Hecker et al. 1995b). Similar hydrogeological conditions caused by quaternary faults have been observed in nearby areas (Wentworth and Yerkes 1971). These mechanisms could explain the abrupt decay of the groundwater table observed at the Balboa Boulevard site and in lieu of any other evidence, the present work adopted the groundwater table originally reported by Holzer et al. (1999).

Hypothesized Ground Failure Mechanisms

Several failure mechanisms have been proposed as causing the observed ground deformations at Balboa Boulevard based on postearthquake reconnaissance efforts in the affected area and simplified analyses. Early hypotheses focused on the dynamic compaction of dry sediments (Day 1996) and coseismic displacements due to secondary faulting (Cruikshank et al. 1996; Johnson et al. 1996; Stewart et al. 1996), but they were later disregarded (Holzer et al. 1999). More recent work has focused on the contributions to the overall ground deformations observed from the saturated soils at Balboa Boulevard. From the units with saturated soils, C and D, all researchers have disregarded Unit D as having contributed to any of the failure mechanisms because it consists of a stronger Pleistocene alluvium (as suggested by SPT blow counts and CPT tip resistance) interpreted to be part of the Saugus Formation (Holzer et al. 1999).

The majority of researchers have attributed ground deformations at Balboa Boulevard to strength loss and deformation in the sand-like (liquefaction) and clay-like (cyclic softening) materials within Unit C. Liquefaction (Holzer et al. 1999; Idriss and Boulanger 2010; Boulanger and Idriss 2015; Cetin et al. 2018) is consistent with a few locations that predominantly contain sand-like soils [e.g., Bal-10 in Figs. 3(b) and 5(a)], while most of the CPT locations mainly suggested the presence of clay-like soils as inferred from SBT and supported by FC and PI. At a system level, it would be unlikely that localized liquefaction alone would have caused such lateral spreading (e.g., Idriss and Boulanger 2008) unless coupled with the failure of other soils in the area. The potential for the cyclic softening of lean clays, consistent with the subsurface conditions of Balboa Boulevard, was recognized by Stewart et al. (1996) and Holzer et al. (1999) and has been observed in prior case studies in the San Fernando Valley (O'Rourke et al. 1992).

Ground surface deformation patterns, specifically extensional and compressional zones, coincided with zones where the groundwater table fell below Unit C [Fig. 3(b)], as indicated by Holzer and Bennett (2007). This observation strengthened the hypothesis that both liquefaction of sand-like soils and cyclic softening of clay-like soils occurred within the saturated portion of Unit C. The compounded effect of localized liquefaction near Bal-10 and cyclic softening of clay-like soils in surrounding areas could have led to the development of a nearly continuous weak path, allowing for the accumulation of shear strains and lateral deformations, and thus a sliding mass failure mechanism, as originally suggested by Stewart et al. (1996). Without disregarding the potential of other failure mechanisms having had minor contributions to the observed deformations, this hypothesized failure mechanism for the Balboa Boulevard case history will be further examined herein.

Nonlinear Deformation Analyses

Two-dimensional NDAs of the Balboa Boulevard case history were performed using the finite difference software FLAC version 8.0 (Itasca 2016) with three objectives: (1) to investigate the failure mechanism leading to ground deformations at Balboa Boulevard; (2) to evaluate the accuracy of the adopted analysis methods, engineering procedures, and state-of-the-art tools to reasonably estimate horizontal ground displacements; and (3) to identify key factors and parameters contributing to earthquake-induced ground deformations at this site.

The Balboa Boulevard numerical model consisted of a 566-m-long 2.6% gradient slope (estimated as the overall gradient based on the boring logs' elevations) with vertical sides. The model had four parallel layers, corresponding to Units A–D, on top of an elastic base. Thicknesses of Units A, B, C, and D were approximately 0.6, 5.0, 4.5, and 3.0 m, respectively, based on findings from Holzer et al. (1999). The numerical model was implemented as an arrangement of quadrilateral zones 1 m wide and variable thickness, depending on the soil unit. Zone thicknesses for Units A, B, C, and D were 0.3, 1.0, 0.25, and 1.0 m, respectively. A smaller thickness was selected for Unit C to better capture the heterogeneity of soils within this unit. The model base is a 1.5-m-thick layer discretized in quadrilateral 1-m-wide, 0.5-m-thick elastic zones. All zone dimensions complied to recommendations by Kuhlemeyer and Lysmer (1973) for the propagation of waves, calculated for the maximum frequency of the motion relevant to the problem at hand ($f = 25$ Hz) and the smallest shear wave velocity ($V_s = 200$ m/s).

Boundary conditions for the static stage of the analyses represented an infinite slope and imposed equal displacements on the left and right sides of the model by attaching the grid points at similar depths from the model surface. Pore water pressure boundary conditions were assigned to be consistent with field observations as presented in Fig. 3(b). For the dynamic stage, free field boundaries were applied on the model sides, which consisted of five columns of elastic zones at each side to provide confinement to adjacent zones. The small strain shear modulus in these elastic columns was reduced by 30% to account for degradation during shaking. A quiet boundary was applied at the bottom of the model together with horizontal and vertical input ground motions converted to shear and normal stresses, respectively. Seepage was allowed during shaking, deformations were assumed to be small for modeling purposes, and a Rayleigh damping of 0.5% centered at a frequency of 1 Hz was included as proven to be sufficient for most applications (Boulanger and Ziotopoulou 2017). The default time step of 2×10^{-5} s for the explicit integration scheme selected by the platform was used for the analyses. Analyses using large deformations instead of small deformations yielded comparable results, and an

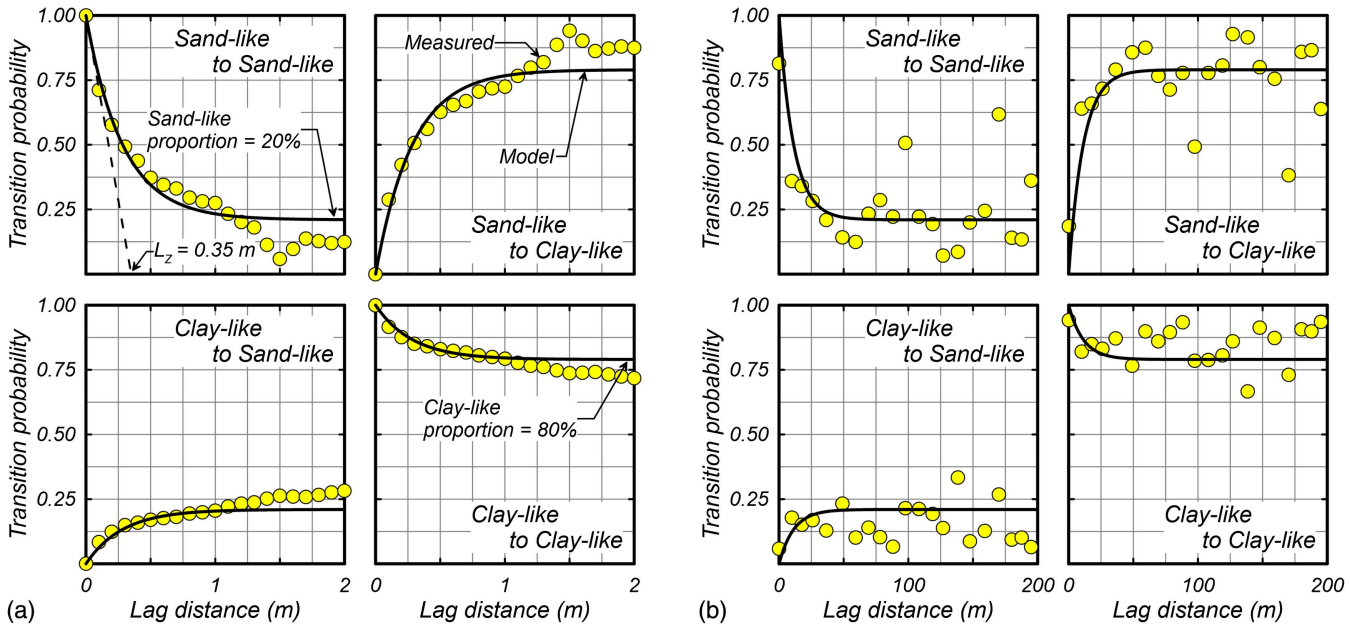

Fig. 7. Measured and modeled transiograms for stratigraphic realizations: (a) transiograms in the vertical direction; and (b) transiograms in the dipping (north–south) direction.

analysis performed with one-half the preceding time step to check the solution stability and results indicated that the default time step was sufficiently small. Similar investigations for other boundary value problem solutions have shown no notable effect of halving or quartering the time step (e.g., Boulanger and Ziotopoulou 2017; Ziotopoulou and Boulanger 2013a, b).

Stratigraphic Models for Heterogeneous Deposit Unit C

Two-dimensional stratigraphic models were developed to capture patterns of the spatial variability of soils within the heterogeneous Unit C. Distinction between sand-like and clay-like soils provided by these models allowed for a realistic modeling of the geologic architecture as well as the appropriate geotechnical characterization and the numerical simulation of these materials.

Transition probability geostatistics implemented in the software T-PROGS were used to generate stratigraphic realizations of Unit C. T-PROGS has the capability to simulate categorical fields conditioned on known locations and inferred elsewhere based on transition probability models determined using Markov chains. Transition probability is the likelihood of transitioning from one category to another (e.g., from sand-like to clay-like soils), thus capturing the ordering of depositional variations. Transition probabilities are defined by sills and mean lengths, which are, respectively, the proportion of a category within the space being modeled and the averaged span of a category in a given direction. The ability of this approach to honor field data and to capture depositional processes makes it a suitable technique to model the Unit C of Balboa Boulevard for NDAs.

Data from all representative CPTs were projected on a single cross section [Fig. 3(b)] and used as conditioning locations for the generation of 20 stratigraphic realizations, referred to as S1–S20. Projecting CPTs was considered acceptable given the geologic environment (alluvial fan deposit), the north–south orientation of the CPTs (likely direction of deposition), and the similarity of separation distances between investigations along and across the alleys. Categories were defined as sand-like and clay-like soils and determined using an I_c cutoff of 2.6, which sets a proportion of 20%–80% for sand-like to clay-like soils. Mean lengths for sand-like and clay-like soils were estimated as 0.35 and 1.2 m in the vertical direction, and 14 and 48 m in the dipping direction. Vertical mean lengths were directly measured from the available CPT data, whose high sampling frequency allowed for an appropriate estimation. Dipping mean lengths were estimated based on the vertical mean lengths and an anisotropic ratio of 40, selected based on measurements by DeGroot (1996) and Phoon and Kulhawy (1996). These researchers found that measured horizontals (i.e., dipping) were generally one order of magnitude larger than the vertical mean lengths, with values ranging from 0.5 to 5 m, and 15 to 50 m, respectively. The estimated mean lengths for Balboa Boulevard were consistent with these researchers' findings. Additionally, an anisotropic ratio of 40 led to a good agreement between the measured and modeled horizontal transiograms. Fig. 7 shows the measured and modeled transiograms with main features indicated, and Fig. 8 shows sample windows of three stratigraphic realizations (S1, S4,

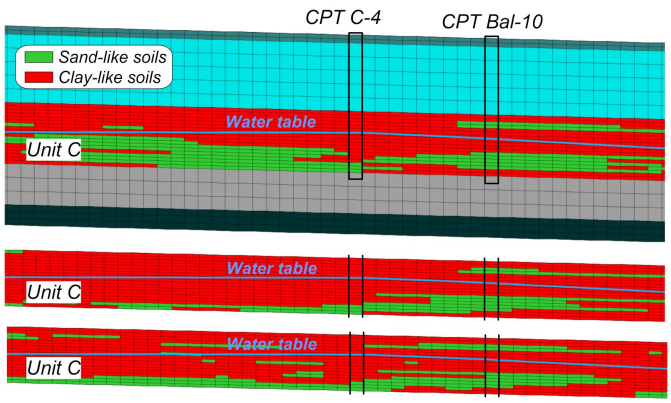

Fig. 8. Sample windows of the Balboa Boulevard numerical domain that are 50 m long illustrating spatial variability of soils ($I_c = 2.6$) within Unit C for three stratigraphic realizations (from top to bottom: S1, S4, and S7). Conditioning CPTs C-4 and Bal-10 indicated in all realizations.

J. Geotech. Geoenviron. Eng., 2021, 147(2): 05020014

and S7) of the Balboa Boulevard numerical domain developed using $I_c = 2.6$. A similar procedure was followed, and suites of equally possible stratigraphic realizations developed for I_c cutoffs of 2.7, 2.8, and 2.9.

Input Ground Motions

The 1994 M_W 6.7 Northridge earthquake was recorded at several sites in the San Fernando Valley (Chang et al. 1996). The location of Balboa Boulevard relative to the epicenter and the propagation of the fault rupture suggested that the site was affected by forward directivity, i.e., a ground motion pulse. Available outcropping recordings were either nonrepresentative of the site conditions at Balboa Boulevard (i.e., no pulse-like motion or too distant to have similar accelerations) or were affected by vibrations of nearby structures and thus disregarded. The RRS is a free surface site located 2.2 km east of Balboa Boulevard [Fig. 9(a)], in a similar location relative to the fault rupture area and epicenter location. The RRS is also located on the north side of the San Fernando Valley and has an inferred common deep deposit with Balboa Boulevard supported by boring logs and V_s profiles (Gibbs et al. 1999; Boore 2003), as schematically illustrated in Fig. 9(b). The RRS recording has been processed by three different teams: Lindvall-Richter-Benuska Associates (1995), Trifunac et al. (1998), and the Pacific Earthquake Engineering Research Center (PEER) (Ancheta et al. 2013). The PEER ground motion recording was selected to be used as the input ground motion for the numerical evaluation of Balboa Boulevard after modification. The PEER ground motion had a recorded duration of about 20 s. Time histories of all the recording components and the Fourier amplitude spectrum of the 228° component are presented in Fig. 9. The PGA, significant duration, and cumulative absolute velocity of the ground motion recordings are presented in Table 1. The 1994 Northridge earthquake was followed by several aftershocks M_W 5 or higher, including a M_W 6.2 event a minute after the mainshock (Dreger 1997; Cultrera et al. 1999). These aftershocks were expected to have had a negligible effect on ground displacements and therefore were not considered for the evaluation.

The RRS provided a free surface recording that required modification to be used as input motion at the base of the NDA model. Deconvolution analysis is typically used to modify free surface recordings (e.g., Mejia and Dawson 2006); however, it can lead to numerical errors (Kramer 1996; Towhata 2008; Pretell et al. 2019) such as unrealistically high accelerations at depth, as was the case

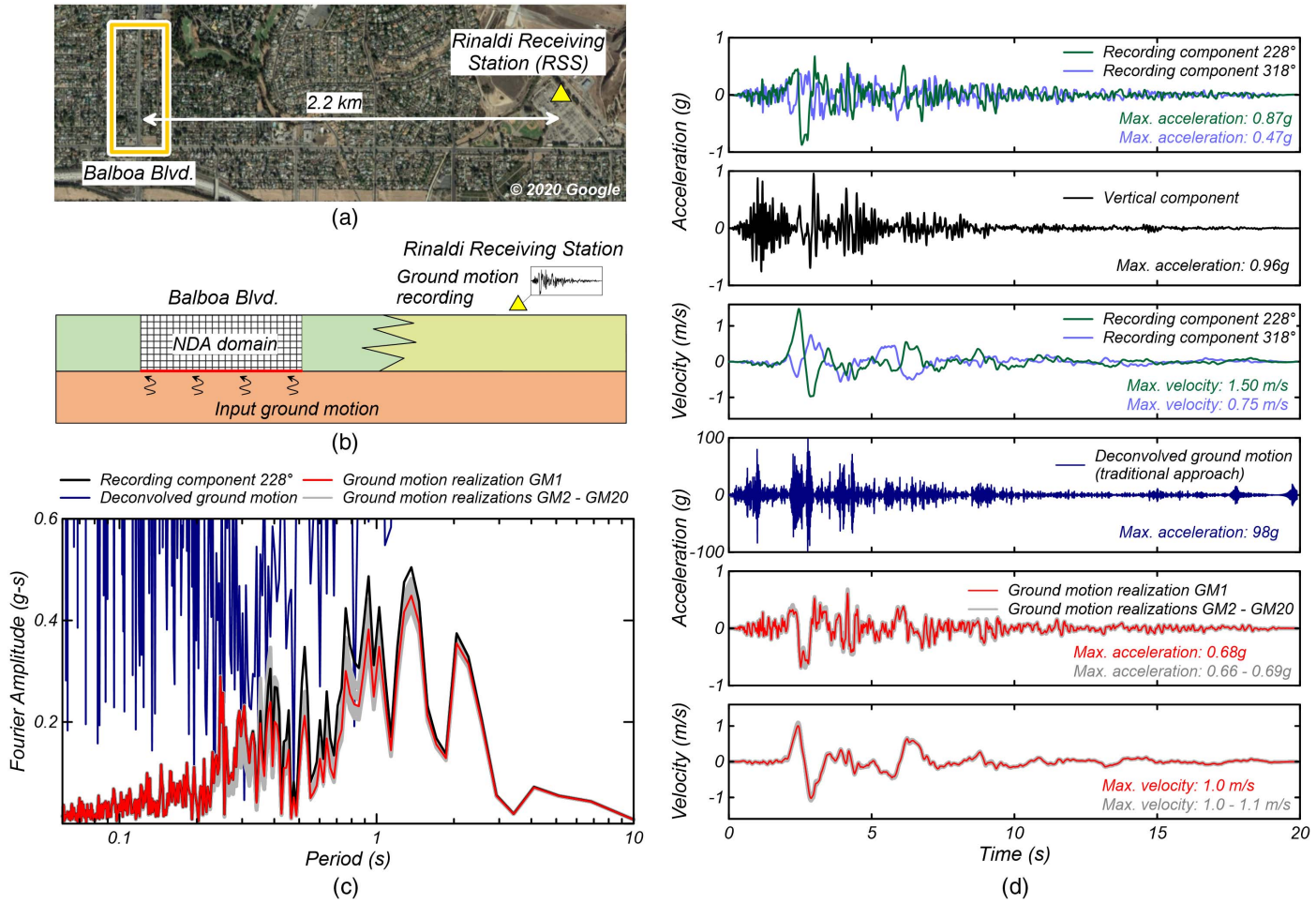

Fig. 9. Ground motions for the Balboa Boulevard NDAs: (a) plan view of the location of the study and reference sites (map data © 2020); (b) schematic of subsurface conditions; (c) Fourier amplitude spectra for free surface RRS recording 228° component, deconvolved ground motion (traditional approach), and ground motion realizations according to Pretell et al. (2019); and (d) from top to bottom: acceleration time histories of the free surface RRS recordings (horizontal and vertical components), velocity time histories of the free surface RRS recordings (horizontal components), acceleration time history of the deconvolved ground motion, acceleration time histories of the input ground motion realizations, and velocity time histories of the input ground motion realizations.

J. Geotech. Geoenviron. Eng., 2021, 147(2): 05020014

Table 1. Main features of the recorded (RRS) and modified ground motions for the NDAs

Ground motion	PGA (g)	Significant duration[a] (s)	Cumulative absolute velocity (m/s)
228° component	0.87	7.23	17.9
318° component	0.47	9.10	15.1
Vertical component	0.96	6.36	14.4
Ground motion realizations	0.66–0.69	7.1–7.4	15.2–16.2

[a]Estimated as the time required to build up from 5% to 95% of the Arias intensity.

for Balboa Boulevard [Figs. 9(c and d)]. The methodology proposed by Pretell et al. (2019) was used to modify the RRS horizontal recording and make it consistent with conditions at the bottom of the model [Fig. 9(b)]. This methodology assumed the absence of nonlinear behavior at the RRS site, as also suggested by postearthquake reconnaissance observations (e.g., Stewart et al. 1994; Davis and Bardet 1994). The recordings were first rotated and the north–south component (i.e., parallel to Balboa Boulevard) used to generate a suite of 20 equally possible input ground motion realizations (referred to as GM1–GM20) following Pretell et al.'s (2019) methodology. All input ground motion realizations carried the ground motion pulse recorded at RRS, as considered appropriate for the numerical evaluation of Balboa Boulevard. Figs. 9(c and d) show these input ground motion realizations in the time and frequency domain. The main features of the input ground motion realizations are presented in Table 1. The developed input ground motions were applied uniformly at the base of the model, neglecting ground motion incoherency, along with the vertical component of the RRS record without any modification. The use of uniform motions was considered appropriate because ground motion incoherency within the span of the model length (about 500 m) is only significant at high frequencies. The input ground motions developed for the NDAs had a high frequency content between 0.5 and 1 Hz, i.e., periods from 1 to 2 s [Fig. 9(c)]. Within this frequency range, seismic waves are expected to be highly coherent, i.e., very similar. For instance, the coherency model proposed by Abrahamson (1993) suggested an expected lagged coherency higher than 0.8 for frequencies lower than 2 Hz and separation distances shorter than 500 m. After the earthquake, significant variability of outcropping ground motions was observed over short distances, mainly caused by the propagation of the fault rupture and the shallow location of the earthquake hypocenter (18.5 km). Based on observations of previous researchers (e.g., Wald and Heaton 1994; Bardet and Davis 1996), there is potential for the ground motion pulse at Balboa Boulevard to be larger. This hypothesis has not been addressed in the present work.

Constitutive Models and Strength Scenarios

The PM4Sand version 3.1 (Ziotopoulou and Boulanger 2016; Boulanger and Ziotopoulou 2017) and PM4Silt version 1.0 (Boulanger and Ziotopoulou 2018, 2019) constitutive models were used to simulate the seismic behavior of sand-like and clay-like soils, respectively. The PM4Sand model is a stress ratio–controlled, critical state–compatible, bounding surface plasticity model developed for earthquake engineering applications simulated in plane-strain conditions. This model has three main input parameters: the apparent relative density (D_R), the shear modulus coefficient (G_o), and the contraction rate parameter (h_{po}). The PM4Silt model builds on the framework of PM4Sand with some modifications to better approximate the response of clays and plastic silts. This model has three main input parameters: the undrained shear strength at critical state, consistent with earthquake loading rates ($s_{u,cs,eq}$), the shear modulus coefficient (G_o), and the contraction rate parameter (h_{po}). Examples of element responses using these models are shown in Boulanger and Ziotopoulou (2017, 2018).

Sand-like and clay-like soils within Unit C were modeled using the PM4Sand and PM4Silt constitutive models. Three sets of input parameters were selected for PM4Sand and PM4Silt, corresponding to the following three strength scenarios: (1) best estimate D_R for sand-like soils and best estimate $s_{u,cs,eq}$ for clay-like soils (hereafter referred to as "best estimate strength scenario"); (2) low D_R for sand-like soils and best estimate $s_{u,cs,eq}$ for clay-like soils (hereafter referred to as "low D_R strength scenario"); and (3) best estimate D_R for sand-like soils and low $s_{u,cs,eq}$ for clay-like soils (hereafter referred to as "low $s_{u,cs,eq}$ strength scenario"). The best estimate strength scenario consisted of median D_R and s_u values observed in the data from field investigations, and both the low D_R and the low $s_{u,cs,eq}$ scenarios addressed possible deviations from the best estimate scenario. While D_R is not typically considered a strength parameter, it is estimated as a function of q_{t1Ncs} and the coefficient C_{dq}; thus, variations of C_{dq} are equivalent to variations of D_R and q_{t1Ncs} for practical purposes. Sand-like soils within Unit C in the best estimate strength scenario were characterized with a $D_R = 50\%$, estimated using the relation by Idriss and Boulanger (2008) with a median $q_{t1Ncs} = 90$ and $C_{dq} = 0.9$. The median q_{t1Ncs} of 90 was also used to estimate the expected cyclic resistance ratio (CRR) using the relation by Boulanger and Idriss (2015). The target CRR corresponding to an $M_W = 7.5$ earthquake at a confinement stress of 1 atm or 101.3 kPa ($CRR_{M7.5,\sigma=1atm}$) was 0.12. The h_{po} was iteratively calibrated to obtain the target CRR in 15 uniform cycles from single-element undrained direct simple shear (DSS) tests simulated in FLAC. Calibrations were performed at various confinement stresses and estimated h_{po} values were interpolated at intermediate stresses for each zone throughout the numerical model. Clay-like soils in the best estimate strength scenario were characterized with the median s_u estimated from field investigations without modification (Fig. 6). This s_u was calibrated against residual strengths estimated from FVTs performed at fast shearing rates, representative of earthquake conditions; thus, it was appropriate to consider $s_{u,cs,eq} \approx s_u = 80$ kPa. The h_{po} parameter of clay-like soils was calibrated so that a reduction of $s_{u,cs,eq}$ in 30% due to degradation is attained after 10 to 30 uniform loading cycles, as observed in results from laboratory cyclic tests on fine-grained soils (Boulanger and Ziotopoulou 2018). The same G_o was used for sand-like and clay-like soils, calculated at each zone such that the overall $V_s = 240$ m/s measured for Unit C is matched, e.g., 1,150 at the middle of Unit C. Default values were used for all other secondary parameters. The low D_R strength scenario only differed from the best estimate scenario in that $D_R = 30\%$ was used for sand-like soils within Unit C, estimated from the median $q_{t1Ncs} = 90$ [Fig. 5(d)] and $C_{dq} = 1.5$, closer to the upper bound of the C_{dq} range (0.64 to 1.7). The low $s_{u,cs,eq}$ strength scenario only differed from the best estimate scenario in that $s_{u,cs,eq} = 50$ kPa was used for clay-like soils, observed to be persistent at similar depths in CPTs Bal-10, Bal-11, Bal-12, and Bal-13b [Figs. 3(b) and 6(d)]. All three strength scenarios shared the same G_o and CRR (sand-like soils), but recalibration of the h_{po} was necessary for each one. A summary of input parameters for the three scenarios of Unit C is presented in Tables 2 and 3.

Units A, B, and D and the model base were modeled with best estimated parameters. The predominantly sand-like Units A and B were modeled using PM4Sand. The D_R values for Units A and B were 32% and 45%, respectively, and G_o values were 5,700 and 1,040 at each unit's middepth, respectively. CRR values for these units were 0.13 and 0.14. Similar to Unit C, h_{po} was calibrated at

Table 2. Main PM4Sand and PM4Silt input parameters, best estimate strength scenario of Unit C

	A	B	C	
	Sand-like	Sand-like	Sand-like	Clay-like
Input parameter	PM4Sand	PM4Sand	PM4Sand	PM4Silt
Corrected tip resistance, q_{t1Ncs}	96	101	89	—
$CRR_{M7.5,\sigma=1atm}$	0.13	0.14	0.12	—
Apparent relative density, D_R (%)[a]	52	52	50	—
Undrained strength, $s_{u,cs,eq}$ (kPa)	—	—	—	82
Shear wave velocity, V_s (m/s)	220	200	240	240
Shear modulus coefficient, G_o[b]	5,700	1,040	1,150	1,150
Contraction rate parameter, h_{po}[b]	0.53	0.06	0.24	70

Note: Default values were used for all secondary parameters as listed in Boulanger and Ziotopoulou (2017, 2018).
[a]Estimated using a median value $C_{dq} = 0.9$.
[b]Estimated at approximately the middle of the unit.

Table 3. Main PM4Sand and PM4Silt input parameters for alternative strength scenarios of Unit C

	Low D_R		Low $s_{u,cs,eq}$	
	Sand-like	Clay-like	Sand-like	Clay-like
Input parameter	PM4Sand	PM4Silt	PM4Sand	PM4Silt
Apparent relative density, D_R (%)	30[a]	—	50	—
Undrained strength, $s_{u,cs,eq}$ (kPa)	—	82	—	50
Contraction rate parameter, h_{po}[b]	2.6	70	0.24	30

Note: All other primary parameters were the same as Table 1, and default values used for all secondary parameters as listed in Boulanger and Ziotopoulou (2017, 2018).
[a]Estimated using $C_{dq} = 1.5$.
[b]Estimated at approximately the middle of the unit.

various confinement levels and interpolated in between. A summary of the input parameters for Units A and B is presented in Table 2. Unit D and the model base were considered elastic materials with small strain shear moduli consistent with field V_s measurements ($V_s = 350$ and 450 m/s, respectively). Hysteretic damping models calibrated against shear modulus reduction curves consistent with sandy soils under high confinement pressures (Darendeli 2001) were additionally assigned to these materials.

Baseline Case Results

This case uses S1 developed using $I_c = 2.6$, GM1, the best estimate strength scenario along with the groundwater table reported by Holzer et al. (1999), an overall ground surface gradient of 2.6%, and the measured V_s. Results from the baseline case at the end of shaking are presented in Fig. 10 along with the observed zones of maximum extension and compression [Fig. 2(d)]. Figs. 10(a–d) show respectively the numerical model, estimated horizontal displacements, shear strains, and excess pore water pressure ratios (r_u) within the saturated portion of Unit C. Fig. 10(e) shows horizontal strains (ε_{xx}) along the surface for all the analyses performed to address potential variations of parameters observed in the data. The horizontal displacements at the surface generally ranged from 20 to 35 cm, and a concentration of shear strains ranging from 10% to 30% and $r_u > 0.5$ was observed within the saturated portion of Unit C. Furthermore, localized liquefaction surrounding CPT Bal-10 (at about the middle of the model) was suggested by shear strains higher than 20% and r_u values ranging from 0.8 to 1 [Figs. 10(c and d)]. Zones of extension and compression, mapped after the earthquake, were captured as depicted by the horizontal strains along the surface presented in Fig. 10(e) for the baseline case and all other analyses carried out as part of the sensitivity analyses, discussed subsequently. Fluctuations of the strains along the surface were consistent with field observations at Balboa Boulevard, e.g., location of zones of maximum extension and compression [Fig. 10(e)], and other lateral spreading cases (Idriss and Boulanger 2008).

Element-level responses can provide insights to the failure mechanism leading to ground deformations at Balboa Boulevard. Three selected zones, one sand-like and two clay-like, of the numerical model were examined with their locations shown in Fig. 11(a). Fig. 11(b) presents the acceleration time history used for the baseline case emphasizing the ground motion pulse at 2 s. Figs. 11(c–h) illustrate the stress–strain responses of the selected sand-like and clay-like zones, identifying the span corresponding to the ground motion pulse. Generally, distinct behaviors were observed before and after the ground motion pulse. Initially, both sand-like and clay-like soils had a similarly stiff response with little degradation (shear strains smaller than 0.1%), as observed in Figs. 11(c, e, and g). This response softened and manifested different patterns upon arrival of the ground motion pulse. The stress–strain response of the sand-like zone exhibited characteristic banana-shaped loops [Fig. 11(d)], typical of sand-like soils experiencing large deformations (i.e., about 0.1% shear strains or larger). The clay-like zone 1 [Fig. 11(f)] experienced loops with larger enclosed areas (indicative of greater energy dissipation and cyclic softening) along with some ratcheting. The stress–strain response of clay-like zone 2 showed stiff responses before and after the ground motion pulse [Figs. 11(g and h)], with a rapid increase in shear strains in between, of about 2.5%, indicative of shear failure of clay-like soils and absence of cyclic softening within this clay-like zone. Observations of these representative zones within the saturated portion of Unit C provide indications that the hypothesized failure mechanism leading to ground deformations at Balboa Boulevard, i.e., liquefaction of sand-like soils along with cyclic softening and shear failure of clay-like soils, may in fact be realistic. Furthermore, these results also indicated the role played by near-fault effects on the observed ground deformations at Balboa Boulevard, as suggested by Stewart et al. (1996).

Results of the baseline case demonstrated that the analyses and engineering procedures (i.e., NDAs combined with transition probability geostatistics, and the user-defined constitutive models PM4Sand and PM4Silt) were able to provide insights into the failure mechanisms leading to ground deformations and to reasonably reproduce ground deformation patterns. The estimated horizontal displacements for the baseline case are lower by 25%–40% compared to the measured field displacements. Sensitivity analyses in the next section will further investigate the effects of various input parameters on these results. Only the maximum ground surface horizontal displacements will be tracked and discussed in the following sections.

Sensitivity Analyses

The baseline case used S1 developed based on $I_c = 2.6$, GM1, and the best estimate strength scenario, along with other best estimate

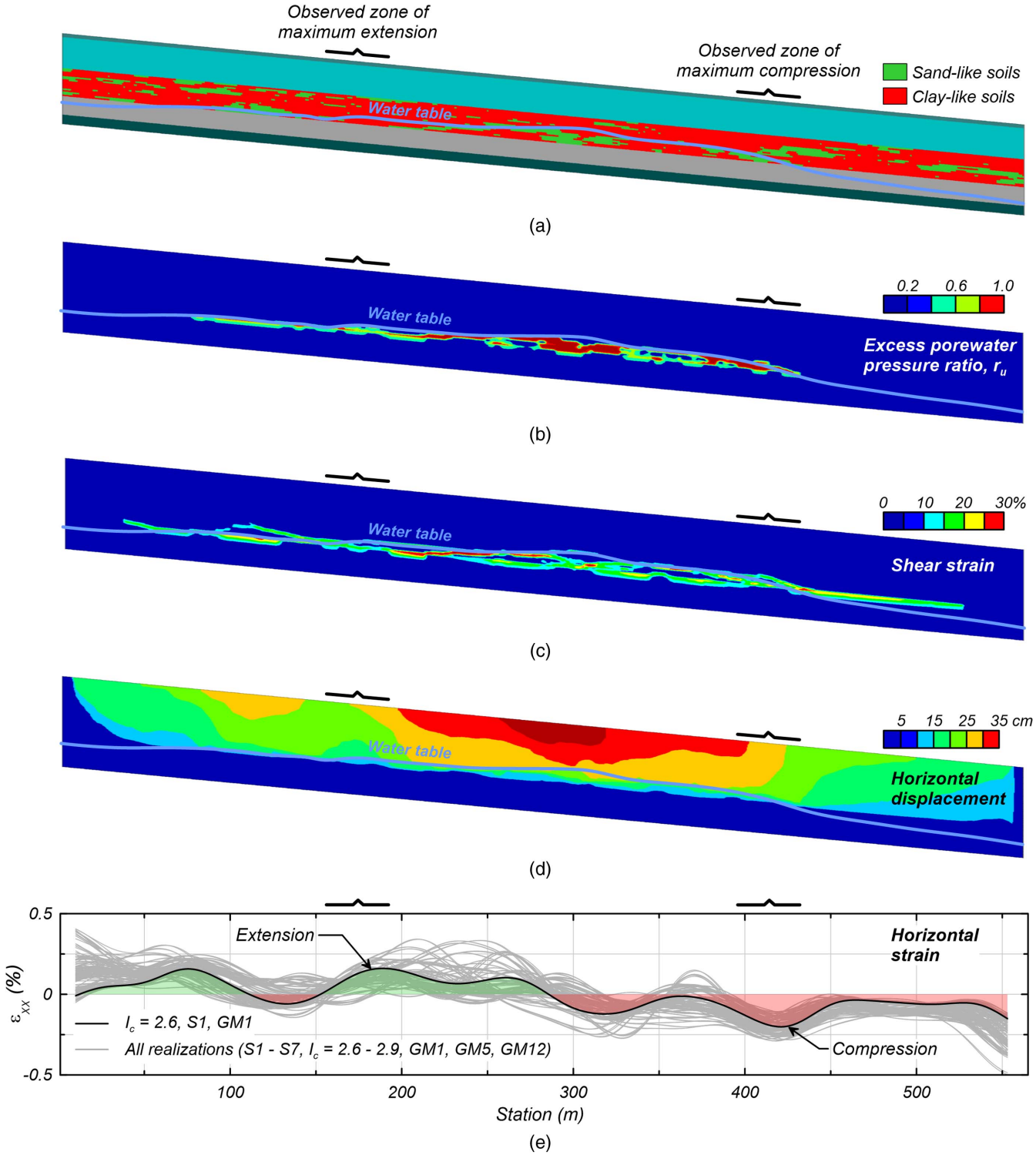

Fig. 10. Results of baseline case at the end of shaking: (a) numerical model; (b) excess pore water pressure ratio (r_u) built up within the saturated portion of Unit C; (c) shear strains developed within the saturated portion of Unit C; (d) horizontal displacements; and (e) smoothed horizontal strains (ε_{xx}) along the surface from baseline case. Results from all additional analyses showing extensional and compressional patterns are also included in (e). The ε_{xx} values were recorded at the top two grid points of the numerical models.

parameters. A number of sensitivity analyses were carried out to account for rational variations in the components (e.g., stratigraphic realizations) and parameters (e.g., D_R, $s_{u,cs,eq}$) used in the baseline case associated with two sources:

1. Variability inherent to subsurface conditions and natural phenomena, e.g., soil stratigraphy, ground motions, variations from median $s_{u,cs,eq}$, groundwater table, ground slope gradient, and V_s.
2. Variability inherent to parameters commonly used in engineering practice that propagate into the estimated soil parameters, i.e., I_c cutoff for the proportion of sand-like and clay-like soils, C_{dq} for D_R.

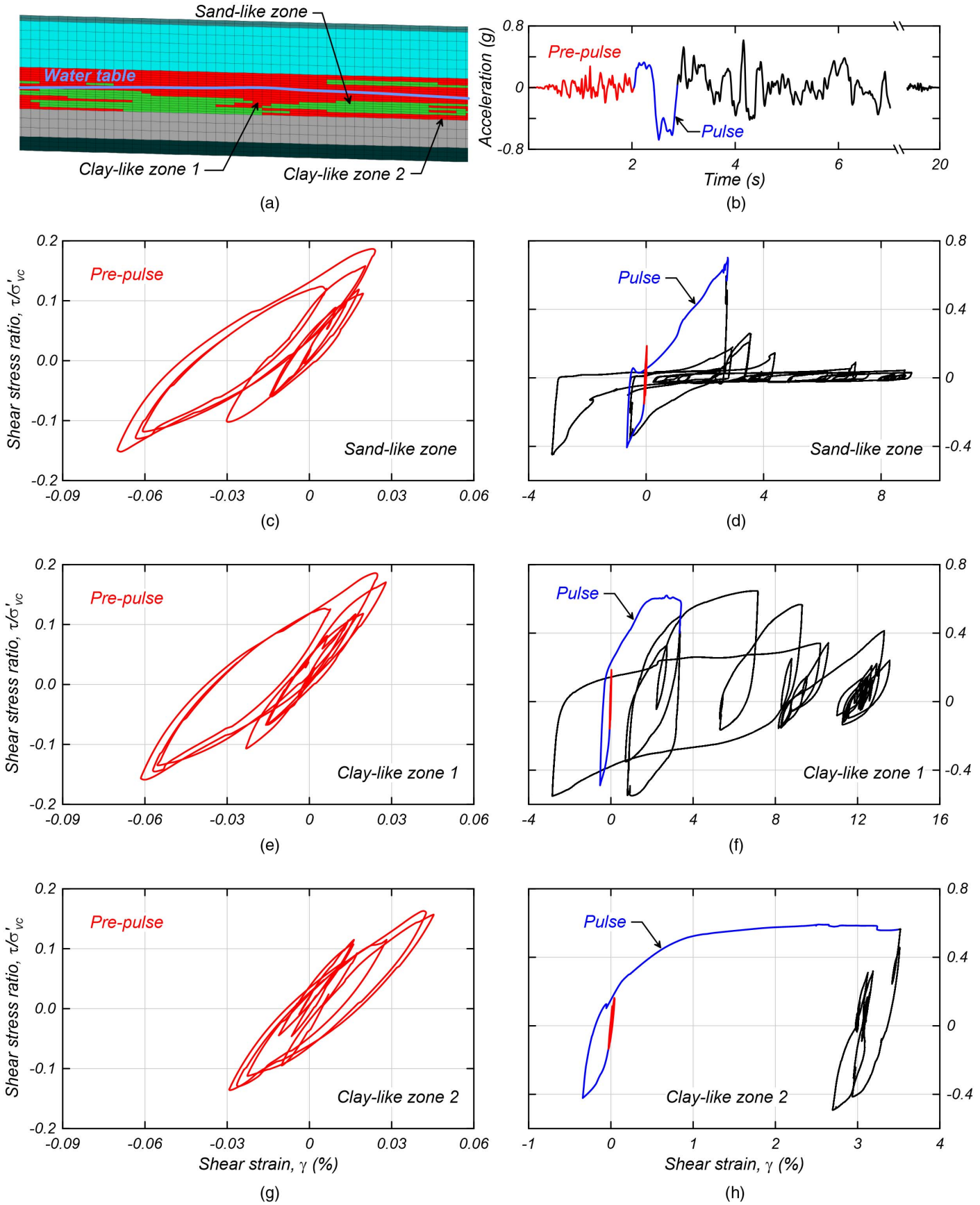

Fig. 11. Effect of ground motion pulse at 2 s on stress–strain response of soils: (a) location of selected sand-like and clay-like zones from stratigraphic realization S1; (b) acceleration time history; (c) prepulse stress–strain response of the sand-like zone; (d) stress–strain response of the sand-like zone during and post pulse; (e) prepulse stress–strain response of clay-like zone 1; (f) stress–strain response of clay-like zone 1 during and post pulse; (g) prepulse stress–strain response of clay-like zone 2; and (h) stress–strain response of clay-like zone 2 during and post pulse.

J. Geotech. Geoenviron. Eng., 2021, 147(2): 05020014

Results from these sensitivity analyses provided insight into the accuracy of NDAs in estimating magnitudes of horizontal displacements and the effect that different modeling parameters have on the estimated ground displacements at Balboa Boulevard. Two sets of parameters were considered for sensitivity analyses with different objectives: (1) soil stratigraphy, input ground motion, I_c cutoff, D_R, and $s_{u,cs,eq}$ were cumulatively varied based on evidence observed in data collected from field investigations; and (2) depth to groundwater table, ground surface gradient, and V_s were individually varied within reasonable ranges selected based on judgment, given the absence of supporting data. The first set of analyses was performed to evaluate the capabilities of numerical tools to accurately estimate horizontal displacements using best estimates for all the parameters considered, whereas the second was meant to identify key parameters on the evaluation of lateral displacements using NDAs. Table 4 summarizes the sensitivity analyses, and lists selected input values and the rationale behind their variations.

Effect of Stratigraphic Realizations

The subsurface stratigraphic model S1 (used in the baseline case) carried uncertainties associated with the heterogeneity of alluvial deposits. This in turn impacted the degree of connectivity of sand-like and clay-like pockets, seams, and layers intimately related to the ultimate estimated ground displacements. Additional NDAs were performed using S2–S20 as well as two cases of homogeneous models, representative of two bounding conditions of Unit C, as commonly done in practice. In all cases, GM1 was used, along with the best estimate strength scenario parameters.

Maximum ground surface horizontal displacements varied from 23 to 37 cm [Fig. 12(a)] with a median of 29 cm, and fell within 25%–50% of the overall measured displacements of 50 cm. The relatively narrow range of maximum displacements suggested that S1–S7 would suffice to cover the range of estimated displacements in subsequent sensitivity analyses. Results from the homogeneous models of sand-like and clay-like soils led to horizontal estimated displacements of 57 and 18 cm, respectively, thus bounding the results from NDAs using realistic stratigraphic models. These results suggested that in the case of forward predictions, honoring the deposit's heterogeneity would likely provide a more accurate estimate of the demands (i.e., ground displacements).

Effect of Input Ground Motions

Input ground motions are a source of large uncertainty, whose influence on the response of geosystems has been studied by several researchers (e.g., Rathje et al. 2010; Bradley 2013; ElGhoraiby and Manzari 2018). The baseline case used GM1. NDAs were performed using GM2–GM20 and the RRS recording without modification. In all cases, S1 was used, along with the best estimate strength scenario.

Maximum ground surface horizontal displacement varied from 29 to 44 cm [Fig. 12(b)] with a median of 34 cm, and are within 10% to 40% of field observations. Similar to the stratigraphic realizations, a relatively narrow range of maximum displacements is observed, and GM1, GM5, and GM12 were selected for subsequent NDAs. Results using the RRS recording led to the significantly higher horizontal displacement of 60 cm, thus emphasizing the importance of appropriate ground motion modification.

Input ground motions for the case history study of Balboa Boulevard were constrained to a specific event and location (e.g., magnitude, site-to-source distance, faulting mechanism). Consequently, these input ground motions led to a relatively narrow range of estimated displacements. It is expected, however, that input ground motions play a more important role or even dominate the seismic response of geosystems in forward predictions.

Effect of I_c Cutoffs

The I_c cutoff determines the proportion of sand-like and clay-like soils at a site. For this study, higher I_c cutoffs led to a greater proportion of sand-like soils in the stratigraphic model and thus a higher degree of connectivity within Unit C. The baseline case used $I_c = 2.6$, which is commonly used in practice (Robertson and Wride 1998), but there is potential for a higher I_c cutoff of 2.9 applicable to Balboa Boulevard. NDAs were performed using suites of seven stratigraphic realizations developed based on I_c cutoffs of 2.7, 2.8, and 2.9. This number of realizations was assumed to be representative of the system response as it was the case for $I_c = 2.6$. The use of different I_c cutoffs led to variations of median tip resistances up to 8% as some soils initially categorized as clay-like shifted to sand-like soils. For these analyses, these variations in tip resistance were considered minor and parameters such as D_R and s_u were not changed. This allowed for the evaluation of the individual effect of sand-like to clay-like proportions on the estimated displacements. In all cases, GM1, GM5, and GM12 were used, along with the best estimate strength scenario. NDAs with uniform models (either sand-like or clay-like soils) were also performed for GM5 and GM12.

Maximum ground surface horizontal displacements using GM1 varied from 25 to 50 cm with a median of 37 cm for $I_c = 2.6$ [Fig. 12(c)], and from 24 to 60 cm with a median of 40 cm for all GM1, GM5, and GM12 [Fig. 12(d)]. These horizontal displacements fell within a range of 50% below and 20% above the measured displacements, and thus were in good agreement with the field observations. Two trends were observed in these results: (1) greater proportions of sand-like soils, caused by higher I_c cutoffs, led to larger horizontal displacements; and (2) higher I_c cutoffs tended to yield similar horizontal displacements, as shown in Fig. 12(c). These trends indicated that the I_c cutoff parameter dominates the stratigraphic models because the influence of stratigraphic realizations on the estimated displacements decreases when

Table 4. Summary of sensitivity analyses, evaluated parameters, input values, and supporting rationale

Parameter evaluated	Input value	Supporting rationale
Stratigraphic realization	S1–S20	Inherent variability of alluvial fan deposits
Ground motion realization	GM1–GM20	Inherent variability of ground motions
I_c cutoff	2.6, 2.7, 2.8, and 2.9	Observations of field and laboratory data
D_R (sand-like soils)	50%, 30%	Variation of C_{dq} to estimate D_R
$s_{u,cs,eq}$ (clay-like soils)	80%, 50 kPa	Observations of field data
Depth to groundwater table	Best estimate, and best estimate ± 1 m	Seasonal variations of groundwater table
V_s	240, 276, 204 m/s	Inherent variability of shear wave velocity
Ground surface gradient	2.6%, 1.6%, 3.6%	Natural variations of surface gradients

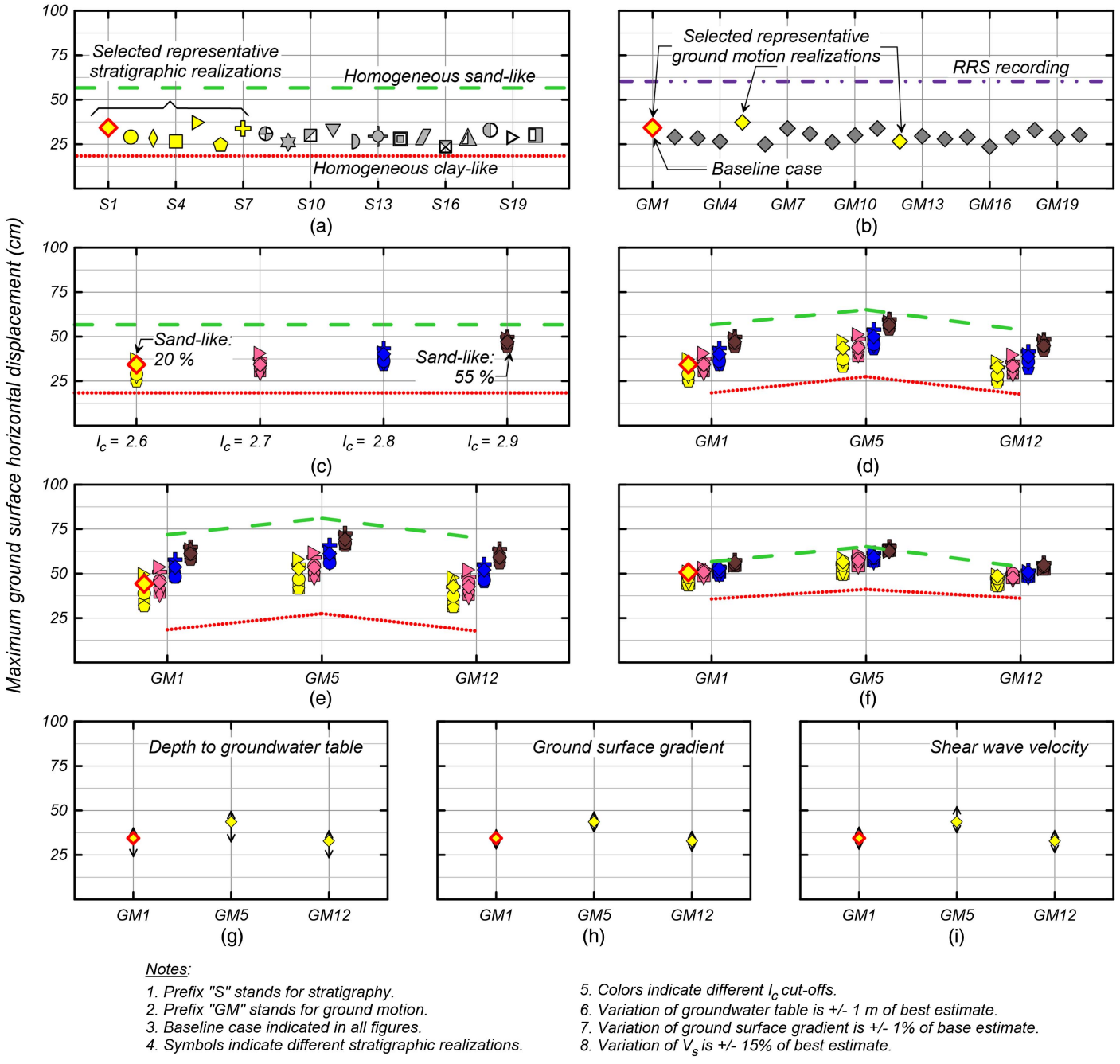

Fig. 12. Effect of selected input parameters on estimated maximum ground surface horizontal displacements: (a) effect of stratigraphic realizations; (b) effect of input ground motion realizations; (c) combined effect of stratigraphic realizations and I_c cutoffs; (d) combined effect of input ground motions, stratigraphic realizations, and I_c cutoffs (best estimate strength scenario); (e) effect of low D_R strength scenario; (f) effect of low $s_{u,cs,eq}$ strength scenario; (g) effect of depth to groundwater table; (h) effect of ground surface gradient; and (i) effect of V_s. An overall lateral displacement of 50 cm was observed after the earthquake.

there is sufficient connectivity among sand-like soils and the more similar the system response of heterogeneous models is to a homogeneous model of sand-like soils.

Effect of Relative Density (D_R)

Relative density D_R is a key parameter controlling the cyclic strength and strain accumulation of sand-like soils and one of the primary input parameters of PM4Sand. This parameter has been estimated using CPT-based correlations, whose uncertainties have been studied (e.g., Jamiolkowski et al. 2003; Hamidi et al. 2013). The possibility of Unit C's sand-like soils having a lower D_R = 30% was addressed by reevaluating all previously discussed models using the set of input parameters corresponding to the low D_R strength scenario.

Maximum ground surface horizontal displacements varied from 31 to 73 cm with a median of 52 cm [Fig. 12(e)]. These horizontal displacements fell within a range of 40% below and 45% above the measured displacements, and thus were in good agreement with field observations. Homogeneous models of sand-like soils yielded

J. Geotech. Geoenviron. Eng., 2021, 147(2): 05020014

displacements as high as 81 cm. These results indicated that, as expected, a lower D_R of sand-like soils led to larger horizontal displacements and a greater spread of the displacements estimated from different stratigraphic realizations compared to previous cases as can be observed by comparing the range of displacements from various realizations corresponding to a single ground motion and I_c cutoff value in Figs. 12(d and e). The spread of displacements indicates that a lower D_R value boosted the influence of the stratigraphic realizations on the estimated displacements as the connectivity of the weaker pockets and seams of sand-like soils becomes critical in the accumulation of lateral displacements.

Effect of Undrained Shear Strength ($s_{u,cs,eq}$)

Undrained shear strength $s_{u,cs,eq}$ is one of the primary input parameters of PM4Silt. Estimated $s_u \approx s_{u,cs,eq}$ values for clay-like soils showed a broad spread with CPTs Bal-10, Bal-11, Bal-12, and Bal-13b having a similar distribution of lower values [Fig. 6(d)]. These CPTs are located together and close to locations where localized liquefaction triggered (i.e., around CPT Bal-10), as shown in Fig. 3(b). It is then likely that this lower $s_{u,cs,eq}$ played a key role in the failure mechanism at Balboa Boulevard. Based on this interpretation, the likely influence of a lower $s_{u,cs,eq} =$ 50 kPa was addressed by reevaluating all the models using the set of input parameters corresponding to the low $s_{u,cs,eq}$ strength scenario.

Maximum ground surface horizontal displacements from these analyses varied from 43 to 65 cm and had a median of 53 cm [Fig. 12(f)]. These horizontal displacements fell within a range of 15% below and 30% above the overall measured displacements, and thus were in good agreement with field observations. Homogeneous models of clay-like soils yielded displacements as low as 36 cm. These results indicated that a lower $s_{u,cs,eq}$ for clay-like soils led to larger horizontal displacements compared to the baseline case and a smaller spread of the displacements estimated from different stratigraphic realizations as compared to previous cases. The convergence of displacements indicates that a lower $s_{u,cs,eq}$ dominates the influence of stratigraphic realizations because the presence of weaker clay-like soils allows for the accumulation of lateral deformations regardless of the degree of connectivity of sand-like pockets and seams.

Additional Sensitivity Analyses

Additional cases evaluated aspects of the analysis (i.e., depth to groundwater table, ground surface gradient, and V_s of Unit C) that were deemed uncertain during the site characterization.

The depth to groundwater table was varied, while keeping its shape, to evaluate the possibility of alternative conditions not captured during the time span of groundwater monitoring. Factors justifying changes of depth to the groundwater table include seasonal fluctuations, local contribution from water leaks prior to the earthquake, and capillary effects (common in fine-grained soils). The position of the groundwater table was lowered and raised 1 m relative to the depths reported by Holzer et al. (1999). NDA results indicated that these changes led to a decrease and increase of the horizontal displacements of about 30% and 18% compared to the baseline case, respectively [Fig. 12(g)].

The ground surface gradient of the numerical model was varied to examine the effects of mildly steeper and flatter ground surface on the estimate ground displacements. Holzer et al. (1999) and SCGC and PG&E (2000) reported, respectively, 1.6% and 2% of surface gradient for the overall area where ground cracking was observed, whereas Stewart et al. (1996) indicated an overall gradient of 2% to 3% for zones of Granada Hills with most severe ground deformations. The baseline ground surface gradient of 2.6% was decreased to 1.6% and increased to 3.6%. NDA results indicated that these changes led to a decrease and an increase of the horizontal displacements of about 5% compared to the baseline case results [Fig. 12(h)].

The V_s was varied to account for the limitations of using data from a single measured V_s profile (at CPT C-3), as suggested by several researchers (e.g., Toro 1995; Griffiths et al. 2016; Stolte and Cox 2019). The value of V_s was decreased and increased by 15% (204 and 276 m/s), which caused a variation of G_o of about 32%. The h_{po} parameter recalibrated for sand-like and clay-like soils. NDA results indicated that these changes led to an increase and a decrease, respectively, of the horizontal displacements of about 20% around results obtained from the baseline case [Fig. 12(i)].

The individual effects of all the evaluated parameters on the estimated displacements appeared to be similar. Fig. 13 is a tornado diagram indicating percentage of variation associated with the increase or decrease in horizontal displacements that each parameter inflicted on the baseline case. From all the parameters, $s_{u,cs,eq}$, the

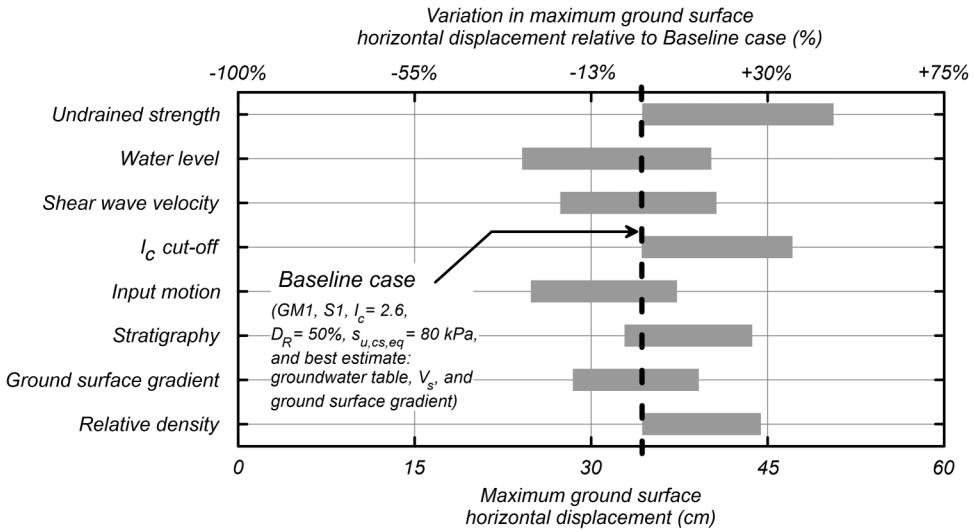

Fig. 13. Individual effect of the NDA main input parameters on estimated maximum ground surface horizontal displacements.

J. Geotech. Geoenviron. Eng., 2021, 147(2): 05020014

depth to groundwater table, V_s, and the I_c cutoff are identified as key parameters for lateral displacements at Balboa Boulevard.

Simplified Analyses

Liquefaction Vulnerability Indexes

LVIs are commonly used in practice because they provide a cost-efficient tool to estimate earthquake-induced damage. LVIs were estimated for Balboa Boulevard and results compared against field observations with the following objectives: (1) to evaluate the extent to which different LVIs agree on their predictions; and (2) to provide insight into the accuracy of LVIs as predictors of earthquake-induced damage.

LVIs were estimated from the CPT-based liquefaction triggering correlations proposed by Boulanger and Idriss (2015) assuming nearly level ground conditions. LVIs were calculated for sand-like soils within the saturated zone of Unit C, which reduced the number of CPTs available for this evaluation from 21 to 12 or less, depending on the I_c cutoff used. Sand-like and clay-like soils were differentiated using I_c cutoffs of 2.6, 2.7, 2.8, and 2.9, consistent with the approach taken for NDAs. Factors of safety against liquefaction, estimated for a PGA of 0.84g, varied from 0.2 to 0.5 in all cases, regardless of the I_c cutoff considered.

The following five LVIs were computed:

- Lateral displacement index (LDI) (Zhang et al. 2004) is an estimation of the maximum liquefaction-induced lateral displacement at the surface, computed by integrating the maximum possible shear strains over depth. Maximum shear strains were estimated using the Yoshimine et al. (2006) expression to approximate the relationship between maximum shear strain and factors of safety against liquefaction developed by Ishihara and Yoshimine (1992). Estimated LDIs ranged from 2 to 110 cm with a median of 17 cm.
- Liquefaction potential index (LPI) (Iwasaki et al. 1978) is an indicator of liquefaction effects at the surface that recognizes the larger influence that shallower soils have on surficial damage. LPIs were estimated as the cumulative depth-weighted function of factors of safety. Estimated LPIs ranged from 0.3 to 9.2 with a median of 1.7.
- Ishihara-inspired liquefaction potential index (LPI_{Ish}) (Maurer et al. 2015) is an alternative version of the LPI, modified to account for the presence of nonliquefiable soil layers (e.g., soil crust) and to better capture the observations by Ishihara (1985) from Japanese earthquakes. LPI_{Ish} values were estimated as the cumulative depth-weighted function of the factors of safety over the liquefiable layer. Estimated LPI_{Ish} values ranged from 0 to 4.6 with a median of 0.8.
- One-dimensional (1D) settlement ($S_{v-1\,D}$) (Zhang et al. 2002) is an estimation of the liquefaction-induced vertical displacements. Settlements were estimated by integrating postliquefaction volumetric strains over depth as proposed by Zhang et al. (2002) and following the recommendations by Ishihara and Yoshimine (1992), approximated by the relation proposed by Yoshimine et al. (2006). Estimated 1D settlements ranged from 0.3 to 9 cm with a median of 1.5 cm.
- Liquefaction severity number (LSN) (van Ballegooy et al. 2014) is a variation of $S_{v-1\,D}$ meant to map damage to structures. LSNs were estimated by integrating a depth-weighted function of volumetric (reconsolidation) strains. Estimated LSNs ranged from 0.25 to 10.7 with a median of 1.7.

Field observations after the earthquake suggested an overall ground displacement of 50 cm and damage that could be reasonably categorized as severe. A summary of estimated LVIs per I_c cutoff is presented in Table 5. Two different trends are observed. First, LPI, LPI_{Ish}, and LSN values suggested none to minor surficial damage according to the liquefaction manifestation severity categories after McLaughlin (2017), developed based on field observations during the Canterbury earthquake sequence (Wotherspoon et al. 2013; Maurer et al. 2014; van Ballegooy et al. 2015; Tonkin & Taylor 2015, 2016). Similarly, estimated $S_{v-1\,D}$ indicated minor surficial damage, based on their similarity with LSN results. Second, LDIs indicated the potential for negligible to significant displacements. LDIs for I_c cutoffs of 2.6 and 2.7 ranged from 2 to 56 cm, thus falling below to slightly below the field observations, whereas LDIs for I_c cutoffs of 2.8 and 2.9 ranged from 5 to 112 cm, widely enveloping the field observations (Table 5). Most of the contribution to the estimated LVIs came from CPT Bal-10 [Fig. 5(a)], which contains most of the sand-like soils within the saturated portion of Unit C along Balboa Boulevard.

Newmark Sliding Block Analyses

The sliding block regression model proposed by Bray and Macedo (2019) was used to calculate seismic-induced displacements at Balboa Boulevard. This methodology follows the framework of Bray and Travasarou (2007) with an additional feature to account for near-fault ground motions (i.e., pulse records), which suits the Balboa Boulevard case history well. Permanent displacements for fault parallel and normal conditions were estimated for 50%, 84%, and 16% probability of exceedance levels. Results from these analyses were compared against measured field displacements.

Permanent displacements were estimated using similar conditions as NDAs. The S1 stratigraphic realization ($I_c = 2.6$) and the homogeneous sand-like and homogeneous clay-like models were used in combination with the three strength scenarios (i.e., best estimate, low D_R, and low $s_{u,cs,eq}$), and GM1, GM5, and GM12. Limit equilibrium analyses were carried out using Spencer's (1967) method to estimate yield accelerations for the three strength scenarios. Sand-like soils within the saturated zone of Unit C were characterized with liquefied strengths estimated using the relation for median mobilized strength ratios during lateral spreading proposed by Olson and Johnson (2008) as a function of the overburden-normalized CPT tip resistance (q_{t1}). For the low D_R strength

Table 5. Estimated liquefaction vulnerability indexes for Balboa Boulevard and interpretation

I_c[a]	FS[b]	LDI (cm)	LPI	LPI_{Ish}	$S_{v-1\,D}$ (cm)	LSN
2.6	0.2–0.5 (liquefaction)	2–25	0.3–4.0 (none to marginal)	0–1.7 (none to marginal)	0.3–3.1	0.3–3.5 (none to marginal)
2.7	0.2–0.5 (liquefaction)	4–56	0.4–5.9 (none to marginal)	0.2–2.8 (none to marginal)	0.4–5.1	0.4–6.0 (none to marginal)
2.8	0.2–0.5 (liquefaction)	5–75	0.4–7.2 (none to marginal)	0.2–3.5 (none to marginal)	0.4–6.5	0.5–7.7 (none to marginal)
2.9	0.2–0.5 (liquefaction)	11–112	0.9–9.2 (none to moderate)	0.5–4.6 (none to marginal)	0.9–8.8	1.0–10.7 (none to marginal)

Note: Interpretation of LVIs' liquefaction manifestation severity categories after McLaughlin (2017).
[a]Sand-like to clay-like proportions for the overall site, $I_c = 2.6$: 20:80, $I_c = 2.7$: 30:70, $I_c = 2.8$: 35:65, and $I_c = 2.9$: 55:45.
[b]Factor of safety against liquefaction (Boulanger and Idriss 2015). Three values with FS > 1 were omitted from the ranges.

scenario, q_{t1} was back-calculated from $D_R = 30\%$ using $C_{dq} = 0.9$, which yielded a value of about $q_{t1Ncs} = 53$. Thus, q_{t1} values for the best estimate and low D_R strength scenarios were respectively 9 and 5.4 MPa; the corresponding estimated postliquefaction strengths (s_u/σ'_{vo}) were 0.16 and 0.11. Clay-like soils were characterized with $s_{u,cs,eq}$ corresponding to each strength scenario, as previously done for NDAs, i.e., $s_{u,cs,eq} = 80$ and 50 kPa. Units A, B, and sand-like soils within Unit C above the groundwater table were characterized with friction angles of 32°, 36°, and 36°, estimated using CPT-based correlations proposed by Kulhawy and Mayne (1990) as previously described.

The sliding surfaces estimated from limit equilibrium analyses were similar for all strength scenarios and consisted of a 9.5-m-thick block running along the lower portion of Unit C and daylighting at the surface near the locations where groundwater level falls deeper into Unit D [Fig. 3(b)]. The V_s of the sliding mass was estimated as the weighted average V_s of Units A to C (220 m/s). The degraded period for the sliding block was about 0.22 s, the spectral accelerations for the three ground motion realizations were 1.45, 1.15, and 1.45g, and peak ground velocities were about 1 m/s in all cases [Fig. 9(d)]. Estimated yield accelerations for S1 under the three best estimate, low D_R, and low $s_{u,cs,eq}$ strength scenarios were 0.31, 0.28, and 0.24g. The corresponding permanent displacements ranged from 9 to 63 cm (median of 23 cm), 11 to 76 cm (median of 28 cm), and 15 to 98 cm (median of 38 cm), with a global median value of 30 cm. Estimated yield accelerations for the homogeneous sand-like model under the best estimate and low D_R strength scenarios were 0.18 and 0.14g. The corresponding permanent displacements ranged from 25 to 155 cm (median of 62 cm), and 38 to 220 cm (median of 92 cm), with a global median value of 75 cm. Finally, estimated yield accelerations for the homogeneous clay-like model under the best estimate and low $s_{u,cs,eq}$ strength scenarios were 0.50 and 0.30g. The corresponding permanent displacements ranged from 3 to 25 cm (median of 8 cm), and 9 to 67 cm (median of 24 cm), with a global median value of 14 cm. These results overall enveloped the observed ground displacements.

Discussion of Capabilities and Limitations of Methods Used

The seismic performance of Balboa Boulevard during the 1994 M_W 6.7 Northridge earthquake was evaluated using (1) NDAs; (2) LVIs; and (3) Newmark sliding block analyses. Results from these three approaches in terms of displacements and surficial damage at Balboa Boulevard were compared and discrepancies discussed.

Various sensitivity analyses were carried out using NDAs for three strength scenarios (best estimate, low D_R, and low $s_{u,cs,eq}$). These analyses yielded median maximum displacements of 40, 52, and 53 cm, respectively, and a global range of 24–73 cm, with a median of 49 cm. NDA results are in good agreement with measured ground displacements at Balboa Boulevard, which were observed to be around 50 cm. Two tendencies were obtained from LVIs: (1) LPI, LPI_{Ish}, $S_{v-1\,\text{D}}$, and LSN generally suggested none to minor surficial damage; and (2) LDIs indicated potential for large displacements, ranging from 2 to 110 cm with a median of 17 cm. Estimated horizontal displacements using Newmark sliding block analyses ranged from 9 to 98 cm (corresponding to 16%–84% probability of exceedance) with a median of 31 cm. Most of the LVIs underestimated surficial damage at Balboa Boulevard, whereas LDIs and Newmark sliding block analyses managed to widely envelope the observed ground deformations with discrepancies in the overall median value. The lower accuracy of simplified methods to assess seismic-induced surficial damage or to estimate ground displacements for this site were attributed to the inherent limitations of these methods (Boulanger et al. 2016). For instance, LVIs considered consequences due to liquefaction of sand-like soils only, thus neglecting contributions from clay-like soils. Overall, Newmark sliding block analyses and NDAs were found better suited for the evaluation of lateral displacements at the site studied using the described modeling procedures.

Concluding Remarks

The seismic performance of Balboa Boulevard during the 1994 M_W 6.7 Northridge earthquake was examined through NDAs using state-of-the-art numerical tools and simplified methods. Subsurface conditions at Balboa Boulevard were evaluated based on the understanding of the geologic setting of the region as well as field and laboratory data from investigation campaigns. The transition probability software T-PROGS was used to generate realistic stratigraphic models that capture the spatial variability of sand-like and clay-like soils. The stratigraphic models were implemented in the finite difference software FLAC and the seismic behavior of sand-like and clay-like soils simulated with the user-defined advanced constitutive models PM4Sand and PM4Silt. Uncertainties associated with the selection of input parameters were examined parametrically. Additional NDAs were carried out to study the individual effect of depth to water table, ground surface gradient, and V_s on ground displacements, and select modeling decisions, adding up to 302 NDAs. Simplifications were made due to the lack of supportive field and laboratory data or limitations in the currently available numerical tools and modeling techniques. These simplifications include neglecting the effect of capillary effects, spatial variability of soil parameters (e.g., D_R and s_u), and bidirectional shaking. These factors were, however, considered minor and were not expected to impact any of the conclusions of the presented work.

The seismic performance of Balboa Boulevard using NDAs accurately reproduced observed ground deformation patterns, with the results suggesting liquefaction of sand-like soils together with cyclic softening and shear failure of clay-like soils as the failure mechanism leading to ground deformations at this site. The compounded effect of localized liquefaction of sand-like soils and softening of clay-like soils allowed for the accumulation of shear strains and lateral deformations. Additionally, high shear stresses associated with near-fault effects, i.e., ground motion pulse, appeared to have triggered or exacerbated nonlinear behavior of soils and ground deformations at Balboa Boulevard and have caused shear failure of clay-like soils. These results recognized the contribution of clay-like soils to ground displacements during earthquakes, typically overlooked when assessing lateral spreading displacements in common practice.

Sensitivity analyses accounting for uncertainties associated with different possible realizations and representative measured or typical values selected as input parameters better enveloped the observed displacements. Results suggested that the modeling of realistic profiles of sand-like and clay-like soils by means of transitional probability geostatistics in combination with advanced constitutive models can provide a more informative range of expected demands in forward predictions. Furthermore, the use of best estimate scenarios based on median values observed in data might not be the most appropriate for the seismic performance of geosystems. Instead, input parameters should be selected based on a hypothesized failure mechanism and ranges of possible values used. Specific to the section of the Balboa Boulevard site studied herein, the

system response was found most sensitive to the individual effects of $s_{u,cs,eq}$, depth to groundwater table, V_s, and I_c cutoff.

Different trends were observed in results from simplified methods. LPI, LPI_{Ish}, $S_{v-1\,D}$, and LSN suggested minor damage, incompatible with field observations, whereas LDI managed to envelope the observed displacements. It is concluded that for complex sites such as Balboa Boulevard (heterogeneous deposit of sand-like and clay-like soils, exposed to pulse-like motions, and a relatively deep groundwater table), LVIs cannot provide much insight into seismic-induced damage. Newmark sliding block analyses were overall consistent with field measurements when used in combination with realistic profiles, and enveloped the field measurements when used in combination with homogeneous models of sand-like and clay-like soils. Inaccuracies of simplified methods to assess seismic-induced damage or to estimate ground displacements at Balboa Boulevard were attributed to the inherent assumptions and limitations these methods carry. Particularly, LVIs account for consequences due to liquefaction of sand-like soils within individual CPTs, but they are challenged by complex subsurface conditions such as those of Balboa Boulevard. In such cases, the seismic performance of geosystems should be evaluated at the system level, work for which NDAs are better suited.

The Balboa Boulevard case history emphasizes the importance of the system-level evaluation of soil deposits and sets an example of sites with apparent innocuous conditions (i.e., a mildly sloping ground on a heterogeneous alluvial fan deposit with a deep groundwater table) that can lead to detrimental consequences upon an earthquake occurrence. Select recommendations pertaining to the seismic evaluation of geosystems are (1) site investigations such as CPTs should extend to the depth of deposits prone to earthquake-induced strength loss; (2) the potential for clay-like soils to contribute to seismic-induced displacements should be considered and evaluated; (3) the potential for groundwater fluctuations should be expected and, when possible, investigated in active tectonic environments because quaternary faults could work as hydraulic barriers; (4) ranges of possible values in the various input parameters should be used in analyzing the seismic performance of geosystems selected based on the potential failure mechanism; and (5) LVIs and Newmark sliding block analyses can provide reasonable estimations provided their applicability has been examined. If potential ground failure can compromise the safety of the overall geosystem and any dependent infrastructure, then more advanced numerical analyses should be carried out.

Data Availability Statement

Some or all data, models, or code generated or used during the study are available upon reasonable request. The manual, dynamic link library, and example calibration files for PM4Sand and PM4Silt are available at https://pm4sand.engr.ucdavis.edu/ and https://pm4silt.engr.ucdavis.edu, respectively. The USGS data along Balboa Boulevard are available at https://earthquake.usgs.gov/research/cpt/data/losangeles/.

Acknowledgments

The authors are grateful to Professors Ross W. Boulanger and Jason T. DeJong for valuable discussions on case history interpretation. Professor Norman A. Abrahamson was instrumental in ground motion development as well as in providing access to the SCGC and PG&E site investigation data. The authors' work also benefited greatly from discussions with Dr. Christopher P. Krage and Professor Graham E. Fogg on transition probability geostatistics. Last but not least, the authors would like to thank Dr. Thomas L. Holzer for sharing his experience on the case history studied herein. The anonymous reviewers provided valuable suggestions for specific improvements, broader discussions, and clarifications that improved the paper. Any opinions or conclusions expressed herein are those of the authors and do not necessarily reflect the views of any of the named people or the represented organizations.

References

Abrahamson, N. A. 1993. "Generation of spatially incoherent strong motion time series." In *Proc., 1st US Seminar on Seismic Evaluation and Retrofit of Steel Bridges*. Berkeley, CA: Univ. of California.

Ancheta, T. D., et al. 2013. *PEER NGA-West2 database*. PEER Rep. No. 2013/03. Richmond, CA: Pacific Earthquake Engineering Research Center.

Bardet, J. P., and C. A. Davis. 1996. "Engineering observations on ground motion at the Van Norman Complex after the 1994 Northridge earthquake." *Bull. Seism. Soc. Am.* 86 (1): 333–349.

Bennett, M. J., D. J. Ponti, J. C. Tinsley, T. L. Holzer, and C. H. Conaway. 1998. *Subsurface geotechnical investigations near sites of ground deformations caused by the January 17, 1994, Northridge, California, earthquake*. Washington, DC: USGS.

Boore, D. M. 2003. *A compendium of P- and S-wave velocities from surface-to-borehole logging: Summary and reanalysis of previously published data and analysis of unpublished data*. Washington, DC: USGS.

Boulanger, R. W. 2019. "Nonlinear dynamic analyses of Austrian dam in the 1989 Loma Prieta earthquake." *J. Geotech. Geoenviron. Eng.* 145 (11): 05019011. https://doi.org/10.1061/(ASCE)GT.1943-5606.0002156.

Boulanger, R. W., and I. M. Idriss. 2015. "CPT-based liquefaction triggering procedure." *J. Geotech. Geoenviron. Eng.* 142 (2): 04015065. https://doi.org/10.1061/(ASCE)GT.1943-5606.0001388.

Boulanger, R. W., I. M. Idriss, and L. H. Mejia. 1995. *Investigation and evaluation of liquefaction related ground displacements at Moss Landing during the 1989 Loma Prieta earthquake*. Rep. No. UCD/CGM-95/02. Davis, CA: Univ. of California.

Boulanger, R. W., D. M. Moug, S. K. Munter, A. B. Price, and J. T. DeJong. 2016. "Evaluating liquefaction and lateral spreading in interbedded sand, silt, and clay deposits using the cone penetrometer." In Vol. 5 of *Proc., Geotechnical and Geography Site Characterisation*, edited by B. Lehane, H. Acosta–Martinez, and R. Kelly. Sydney, Australia: Australian Geomechanics Society.

Boulanger, R. W., S. K. Munter, C. P. Krage, and J. T. DeJong. 2019. "Liquefaction evaluation of interbedded soil deposit: Çark Canal in 1999 M7.5 Kocaeli earthquake." *J. Geotech. Geoenviron. Eng.* 145 (9): 05019007. https://doi.org/10.1061/(ASCE)GT.1943-5606.0002089.

Boulanger, R. W., and K. Ziotopoulou. 2017. *PM4Sand (version 3.1): A sand plasticity model for earthquake engineering applications*. Rep. No. UCD/CGM-17/01. Davis, CA: Univ. of California.

Boulanger, R. W., and K. Ziotopoulou. 2018. *PM4Silt (version 1): A silt plasticity model for earthquake engineering applications*. Rep. No. UCD/CGM-18/01. Davis, CA: Univ. of California.

Boulanger, R. W., and K. Ziotopoulou. 2019. "A constitutive model for clays and plastic silts in plane-strain earthquake engineering applications." *Soil Dyn. Earthquake Eng.* 127: 105832.

Bradley, B. A. 2013. "A critical examination of seismic response uncertainty analysis in earthquake engineering." *Earthquake Eng. Struct. Dyn.* 42 (11): 1717–1729. https://doi.org/10.1002/eqe.2331.

Bray, J. D., and R. Luque. 2017. "Seismic performance of a building affected by moderate liquefaction during the Christchurch earthquake." *Soil Dyn. Earthquake Eng.* 102 (Nov): 99–111. https://doi.org/10.1016/j.soildyn.2017.08.011.

Bray, J. D., and J. Macedo. 2019. "Procedure for estimating shear-induced seismic slope displacement for shallow crustal earthquakes." *J. Geotech. Geoenviron. Eng.* 145 (12): 04019106. https://doi.org/10.1061/(ASCE)GT.1943-5606.0002143.

Bray, J. D., and T. Travasarou. 2007. "Simplified procedure for estimating earthquake-induced deviatoric slope displacements." *J. Geotech. Geoenviron. Eng.* 133 (4): 381–392. https://doi.org/10.1061/(ASCE)1090-0241(2007)133:4(381).

Cetin, K. O., R. B. Seed, R. E. Kayen, R. E. Moss, H. Tolga Bilge, M. Ilgac, and K. Chowdhury. 2018. "SPT-based probabilistic and deterministic assessment of seismic soil liquefaction triggering hazard." *Soil Dyn. Earthquake Eng.* 115 (Dec): 698–709. https://doi.org/10.1016/j.soildyn.2018.09.012.

Chaloulos, Y., A. Giannakou, V. Drosos, P. Tasiopoulou, J. Chacko, and S. De Wit. 2019. "Shallow foundation liquefaction-induced settlements of residential buildings due to man-induced earthquakes." In *Proc., 7th Int. Conf. on Earthquake Geotechnical Engineering (ICEGE)*, edited by F. Silvestri and N. Moraci, 1689–1697. London: Taylor & Francis. https://www.taylorfrancis.com/books/9780429031274.

Chameau, J. L. A., G. W. Clough, and J. D. Frost. 1998. "Liquefaction characteristics of San Francisco bayshore fills." In *The Loma Prieta, California, earthquake of October 17, 1989—Liquefaction*, edited by T. L. Holzer, 9–24. Washington, DC: USGS.

Chang, S. W., J. D. Bray, and R. B. Seed. 1996. "Engineering implications of ground motions from the Northridge earthquake." *Bull. Seismol. Soc. Am.* 86 (1): 270–288.

Cruikshank, K. M., A. M. Johnson, R. W. Fleming, and R. Jones. 1996. *Winnetka deformation zone: Surface expression of coactive slip on a blind fault during the Northridge earthquakesequence, California*. Washington, DC: USGS.

Cultrera, G., D. M. Boore, W. B. Joyner, and C. M. Dietel. 1999. "Nonlinear soil response in the vicinity of the Van Norman Complex following the 1994 Northridge, California, earthquake." *Bull. Seismol. Soc. Am.* 89 (5): 1214–1231.

Darby, K. M., R. W. Boulanger, J. T. DeJong, and J. D. Bronner. 2019. "Progressive changes in liquefaction and cone penetration resistance across multiple shaking events in centrifuge tests." *J. Geotech. Geoenviron. Eng.* 145 (3): 04018112. https://doi.org/10.1061/(ASCE)GT.1943-5606.0001995.

Darendeli, M. B. 2001. "Development of a new family of normalized modulus reduction and material damping curves." Ph.D. dissertation, Dept. of Civil, Architectural, and Environmental Engineering, Univ. of Texas at Austin.

Davis, C. A., and J. P. Bardet. 1994. "Geotechnical observations at the Van Norman Complex after the 1994 Northridge earthquake." In *Proc., 5th Japan–US Workshop on Earthquake Resistant Design of Lifeline Facilities and Countermeasures against Soil Liquefaction*, edited by T. O'Rourke and M. Hamada, 63–78. Buffalo, NY: National Center for Earthquake Engineering Research. http://65.182.2.246/docum/crid/Diciembre2004/pdf/eng/doc7452/doc7452.htm.

Day, R. W. 1996. "Damage due to Northridge earthquake-induced settlement of clayey fill." *Environ. Eng. Geosci.* 2 (1): 99–105. https://doi.org/10.2113/gseegeosci.II.1.99.

DeGroot, D. J. 1996. "Analyzing spatial variability of in situ soil properties." In Vol. 1 of *Proc., Uncertainty '96, Uncertainty in the Geologic Environment: From Theory to Practice*, edited by C. Shackelford, P. Nelson, and M. Roth, 210–238. Reston, VA: ASCE.

Dreger, D. 1997. "The large aftershocks of the Northridge earthquake and their relationship to mainshock slip and fault-zone complexity." *Bull. Seismol. Soc. Am.* 87 (5): 1259–1266.

ElGhoraiby, M. A., and M. T. Manzari. 2018. "Effects of variability in base excitation on the response of liquefiable heterogeneous sloping ground." In *Proc., Geotechnical Earthquake Engineering Soil Dynamics V*, edited by S. Brandenberg and M. Manzari, 217–226. Reston, VA: ASCE. https://doi.org/10.1061/9780784481455.021.

El-Sekelly, W., T. Abdou, R. Dobry, and J. H. Steidl. 2018. "Field and experimental evidence on the effect of preshaking history on the liquefaction resistance of silty sand deposits." In *Proc., Geotechnical Earthquake Engineering Soil Dynamics V*, edited by S. Brandenberg and M. Manzari, 255–263. Reston, VA: ASCE. https://doi.org/10.1061/9780784481455.025.

Gibbs, J. F., J. C. Tinsley, D. M. Boore, and W. B. Joyner. 1999. *Seismic velocities and geological conditions at twelve sites subjected to strong ground motion in the 1994 Northridge, California, earthquake: A revision of OFR 96-740*. Washington, DC: USGS.

Griffiths, S. C., B. R. Cox, E. M. Rathje, and D. P. Teague. 2016. "Surface-wave dispersion approach for evaluating statistical models that account for shear-wave velocity uncertainty." *J. Geotech. Geoenviron. Eng.* 142 (11): 04016061. https://doi.org/10.1061/(ASCE)GT.1943-5606.0001552.

Hamidi, B., S. Varaksin, and H. Nikraz. 2013. "Relative density correlations are not reliable criteria." *Proc. Inst. Civ. Eng. Ground Improv.* 166 (14): 196–208. https://doi.org/10.1680/grim.11.00016.

Hecker, S., D. J. Ponti, C. D. Garvin, and J. C. Hamilton. 1995a. "Characteristics and origin of ground deformation produced in Granada Hills and Mission Hills during the January 17, 1994 Northridge, California, earthquake." In *The Northridge, California, earthquake of 17 January 1994*, edited by M. Woods and W. Sieple, 111–131. Sacramento, CA: California Dept. of Conservation.

Hecker, S., D. J. Ponti, C. D. Garvin, T. J. Powers, T. E. Fumal, J. C. Hamilton, R. V. Sharp, M. J. Rymer, C. S. Prentice, and F. R. Cinti. 1995b. *Ground deformation in Granada Hills and Mission Hills resulting from the January 17, 1994, Northridge, California, earthquake*. Washington, DC: USGS.

Holzer, T. L., and M. J. Bennett. 2007. "Geologic and hydrogeologic controls of boundaries of lateral spreads: Lessons from USGS liquefaction case histories." In *Proc.,* 1st *North American Landslide Conf.*, edited by V. Schaefer, R. Schuster, and A. Turner, 502–522. Zanesville, OH: Association of Environmental and Engineering Geologists.

Holzer, T. L., M. J. Bennett, D. J. Ponti, and J. C. Tinsley III. 1999. "Liquefaction and soil failure during 1994 Northridge earthquake." *J. Geotech. Geoenviron. Eng.* 125 (6): 438–452. https://doi.org/10.1061/(ASCE)1090-0241(1999)125:6(438).

Holzer, T. L., M. J. Bennett, J. C. Tinsley, D. J. Ponti, and R. V. Sharp. 1996. "Causes of ground failure in alluvium during the Northridge, California, and earthquake of January 17, 1994." In *Proc., 6th Japan–US Workshop on Earthquake Resistant Design of Lifeline Facilities and Countermeasures against Soil Liquefaction*, edited by M. Hamada and T. O'Rourke, 345–360. Buffalo, NY: National Center for Earthquake Engineering Research.

Holzer, T. L., and T. L. Youd. 2007. "Liquefaction, ground oscillation, and soil deformation at the wildlife array, California." *Bull. Seismol. Soc. Am.* 97 (3): 961–976. https://doi.org/10.1785/0120060156.

Idriss, I. M., and R. W. Boulanger. 2003. "Estimating K_α for use in evaluating cyclic resistance of sloping ground." In *Proc., 8th US–Japan Workshop on Earthquake Resistant Design of Lifeline Facilities and Countermeasures against Soil Liquefaction*, edited by M. Hamada, J. Bardet, and T. O'Rourke, 449–468. Buffalo, NY: Multidisciplinary Center for Earthquake Engineering Research.

Idriss, I. M., and R. W. Boulanger. 2008. *Soil liquefaction during earthquakes*. Oakland, CA: Earthquake Engineering Research Institute.

Idriss, I. M., and R. W. Boulanger. 2010. *SPT-based liquefaction triggering procedures*. Rep. No. UCD/CGM–10/02. Davis, CA: Univ. of California.

Ishihara, K. 1985. "Stability of natural deposits during earthquakes." In *Proc., 11th Int. Conf. on Soil Mechanics and Foundation Engineering*, 321–376. Rotterdam, Netherlands: A.A. Balkema.

Ishihara, K., and M. Yoshimine. 1992. "Evaluation of settlements in sand deposits following liquefaction during earthquakes." *Soils Found.* 32 (1): 173–188. https://doi.org/10.3208/sandf1972.32.173.

Itasca. 2016. *FLAC, Fast Lagrangian Analysis of Continua, user's guide*. Minneapolis: Itasca Consulting Group.

Iwasaki, T., F. Tatsuoka, K. Tokida, and S. Yasuda. 1978. "A practical method for assessing soil liquefaction potential based on case studies at various sites in Japan." In *Proc., 2nd Int. Conf. on Microzonation*, 885–896. Washington, DC: Engineering and Applied Science National Science Foundation.

Jamiolkowski, M., D. C. F. Lo Presti, and M. Manassero. 2003. "Evaluation of relative density and shear strength of sands from CPT and DMT." In *Soil Behavior and Soft Ground Construction*, Geotechnical Special Publication 119, edited by J. Germaine, T. Sheahan, and R. Whitman, 201–238. Reston, VA: ASCE. https://doi.org/10.1061/40659(2003)7.

Johnson, A. M., R. M. Fleming, K. M. Cruikshank, and R. F. Packard. 1996. *Coactive fault of the Northridge earthquake—Granada Hills area, California*. Washington, DC: USGS.

Kiernan, M., and J. Montgomery. 2018. "Numerical simulations of the Fourth Avenue landslide considering strain-softening." In *Proc., Geotechnical Earthquake Engineering Soil Dynamics V*, edited by S. Brandenberg and M. Manzari, 67–78. Reston, VA: ASCE. https://doi.org/10.1061/9780784481486.008.

Kramer, S. L. 1996. *Geotechnical earthquake engineering*. Upper Saddle River, NJ: Prentice Hall.

Kuhlemeyer, R. L., and J. Lysmer. 1973. "Finite element method accuracy for wave propagation problems." *J. Soil Mech. Found. Div.* 99 (5): 421–427.

Kulhawy, F. H., and P. W. Mayne. 1990. *Manual on estimating soil properties for foundation design*. Palo Alto, CA: Electrical Power Research Institute.

LABE (Los Angeles Bureau of Engineering). 1995. *Northridge earthquake horizontal movement study.* Los Angeles: LABE.

Ladd, C. C. 1991. "Stability evaluation during staged construction." *J. Geotech. Eng.* 117 (4): 540–615. https://doi.org/10.1061/(ASCE)0733-9410(1991)117:4(540).

Ladd, C. C., and R. Foott. 1974. "New design procedure for stability of soft clays." *J. Geotech. Eng. Div.* 100 (7): 763–786.

Lindvall-Richter-Benuska Associates. 1995. *Processed LADWP power system strong-motion records for the Northridge, California, earthquake of January 17, 1994*. Los Angeles: Lindvall-Richter-Benuska Associates.

Los Angeles County. 1990. *Technical appendix to the safety element of the Los Angeles County general plan, hazard reduction in Los Angeles County.* Los Angeles: Dept. of Regional Planning.

Lunne, T., H. P. Christofferson, and T. I. Tjelta. 1985. "Engineering use of the piezocone data in the North Sea clays." In *Proc., Int. Conf. on Soil Mechanics and Foundation Engineering*, 907–913. Rotterdam, Netherlands: A.A. Balkema.

Luque, R., and J. D. Bray. 2017. "Dynamic analyses of two buildings founded on liquefiable soils during the Canterbury earthquake sequence." *J. Geotech. Geoenviron. Eng.* 143 (9): 04017067. https://doi.org/10.1061/(ASCE)GT.1943-5606.0001736.

Luque, R., and J. D. Bray. 2020. "Dynamic soil-structure interaction analyses of two important structures affected by liquefaction during the Canterbury earthquake sequence." *Soil Dyn. Earthquake Eng.* 133 (Jun): 106026. https://doi.org/10.1016/j.soildyn.2019.106026.

Maurer, B. W., R. A. Green, M. Cubrinovski, and B. A. Bradley. 2014. "Evaluation of the liquefaction potential index for assessing liquefaction hazard in Christchurch, New Zealand." *J. Geotech. Geoenviron. Eng.* 140 (7): 04014032. https://doi.org/10.1061/(ASCE)GT.1943-5606.0001117.

Maurer, B. W., R. A. Green, and O. S. Taylor. 2015. "Moving towards an improved index for assessing liquefaction hazard: Lessons from historical data." *Soils Found.* 55 (4): 778–787. https://doi.org/10.1016/j.sandf.2015.06.010.

McLaughlin, K. A. 2017. "Investigation of false-positive liquefaction case history sites in Christchurch, New Zealand." M.Sc. thesis, Dept. of Civil, Architectural, and Environmental Engineering, Univ. of Texas at Austin.

Mejia, L. H., and E. W. Dawson. 2006. "Earthquake deconvolution for FLAC." In *Proc., 4th Int. FLAC Symp. on Numerical Modeling in Geomechanics*, edited by O. Hart and R. Varona, 211–219. Madrid, Spain: Itasca Consulting Group.

Mesri, G. 1975. "Discussion on the 'New design procedure for stability of soft clays' by C. C. Ladd and R. Foott." *J. Geotech. Eng. Div.* 101 (4): 409–412.

Mitchell, J., and K. Soga. 2005. *Fundamentals of soil behavior.* Hoboken, NJ: Wiley.

Montgomery, J., R. W. Boulanger, and K. Ziotopoulou. 2017. "Effects of spatial variability on the seismic response of the Wildlife Liquefaction Array." In *Proc., Performance Based Design in Earthquake Geotechnical Engineering*, edited by M. Taiebat, et al. London: International Society for Soil Mechanics and Geotechnical Engineering.

Olson, S. M., and C. I. Johnson. 2008. "Analyzing liquefaction-induced lateral spreads using strength ratios." *J. Geotech. Geoenviron. Eng.* 134 (8): 1035–1049. https://doi.org/10.1061/(ASCE)1090-0241(2008)134:8(1035).

O'Rourke, T. D., and M. C. Palmer. 1994. *The Northridge, California earthquake of January 17, 1994: Performance of gas transmission pipelines*. Buffalo, NY: National Center for Earthquake Engineering Research.

O'Rourke, T. D., B. L. Roth, and M. Hamada. 1992. "Large ground deformations and their effect on lifeline facilities: 1971 San Fernando earthquake." In *Proc., Case Histories of Liquefaction and Lifeline Performance During Past Earthquakes*, edited by T. O'Rourke and M. Hamada. Buffalo, NY: National Center for Earthquake Engineering Research.

Phoon, K.-K., and F. H. Kulhawy. 1996. "On quantifying inherent soil variability." In Vol. 1 of *Proc., Uncertainty '96, Uncertainty in the Geologic Environment: From Theory to Practice*, edited by C. Shackelford, P. Nelson, and M. Roth, 326–340. New York: ASCE.

Pretell, R., K. Ziotopoulou, and N. Abrahamson. 2019. "Methodology for the development of input motions for nonlinear deformation analyses." In *Proc., 7th Int. Conf. on Earthquake Geotechnical Engineering (ICEGE)*, edited by F. Silvestri and N. Moraci, 4564–4571. London: Taylor & Francis.

Rathje, E. M., A. R. Kottke, and W. L. Trent. 2010. "Influence of input motion and site property variabilities on seismic site response analysis." *J. Geotech. Geoenviron. Eng.* 136 (4): 607–619. https://doi.org/10.1061/(ASCE)GT.1943-5606.0000255.

Robertson, P. K. 2009. "Interpretation of cone penetration tests—A unified approach." *Can. Geotech. J.* 46 (11): 1137–1355. https://doi.org/10.1139/T09-065.

Robertson, P. K. 2010. "Estimating in situ soil permeability from CPT & CPTu." In *Proc.,* 2nd *Int. Symp. on Cone Penetration Testing (CPT'10)*, edited by J. Mitchell. Signal Hill, CA: Gregg Drilling & Testing.

Robertson, P. K. 2013. "Interpretation of in-situ tests—Some insights." In *Geotechnical and geophysical site characterization 4*. London: Taylor & Francis.

Robertson, P. K., and C. E. Wride. 1998. "Evaluating cyclic liquefaction potential using the cone penetration test." *Can. Geotech. J.* 35 (3): 442–459. https://doi.org/10.1139/t98-017.

SCGC and PG&E (Southern California Gas Company and Pacific Gas and Electric Company). 2000. *Gas pipeline performance in the Northridge* earthquake—Geologic*, geotechnical, and pipeline investigations*. Los Angeles: SCGC and PG&E.

Spencer, E. 1967. "A method of analysis of the stability of embankments assuming parallel inter-slice forces." *Géotechnique* 17 (1): 11–26. https://doi.org/10.1680/geot.1967.17.1.11.

Stewart, J. P., J. D. Bray, R. B. Seed, and N. Sitar. 1994. *Preliminary report on the principal geotechnical aspects of the January 17, 1994 Northridge earthquake*. Rep. No. UCB/EERC-94/08. Berkeley, CA: Univ. of California.

Stewart, J. P., R. B. Seed, and J. D. Bray. 1996. "Incidents of ground failure from the 1994 Northridge earthquake." *Bull. Seismol. Soc. Am.* 86 (1): 300–318.

Stolte, A. C., and B. R. Cox. 2019. "Towards consideration of epistemic uncertainty in shear–wave velocity measurements obtained via seismic cone penetration testing (SCPT)." *Can. Geotech. J.* 57 (1): 48–60. https://doi.org/10.1139/cgj-2018-0689.

Sturm, A. P. 2019. "On the liquefaction potential of gravelly soils: Characterization, triggering and performance." Ph.D. dissertation, Dept. of Civil and Environmental Engineering, Univ. of California, Davis.

Tasiopoulou, P., K. Ziotopoulou, F. Humire, A. Giannakou, J. Chacko, and T. Travasarou. 2019. "Development and implementation of semiempirical framework for modeling postliquefaction shear deformation accumulation in sands." *J. Geotech. Geoenviron. Eng.* 146 (1): 04019120. https://doi.org/10.1061/(ASCE)GT.1943-5606.0002179.

Tonkin & Taylor. 2015. *Canterbury earthquake sequence: Increased liquefaction vulnerability assessment methodology.* Wellington, New Zealand: Earthquake Commission.

Tonkin & Taylor. 2016. *Practical implications of increased liquefaction vulnerability.* Wellington, New Zealand: Earthquake Commission.

Toro, G. R. 1995. *Probabilistic models of the site velocity profiles for generic and site-specific ground-motion amplification studies*. Rep. No. 779574. Upton, NY: Brookhaven National Laboratory.

Towhata, I. 2008. *Geotechnical earthquake engineering*. Berlin: Springer.

Trifunac, M. D., M. I. Todorovska, and V. W. Lee. 1998. "The Rinaldi strong motion accelerogram of the Northridge, California earthquake of 17 January 1994." *Earthquake Spectra* 14 (1): 225–239. https://doi.org/10.1193/1.1585997.

van Ballegooy, S., R. A. Green, J. Lees, F. Wentz, and B. W. Maurer. 2015. "Assessment of various CPT based liquefaction severity index frameworks relative to the Ishihara (1985) H_1–H_2 boundary curves." *Soil Dyn. Earthquake Eng.* 79 (2): 347–364. https://doi.org/10.1016/j.soildyn.2015.08.015.

van Ballegooy, S., P. Malan, V. Lacrosse, M. E. Jacka, M. Cubrinovski, J. D. Bray, T. D. O. O'Rourke, S. A. Crawford, and H. Cowan. 2014. "Assessment of liquefaction-induced land damage for residential Christchurch." *Earthquake Spectra* 30 (1): 31–55. https://doi.org/10.1193%2F031813EQS070M.

Wald, D. J., and T. H. Heaton. 1994. *A dislocation model of the 1994 Northridge, California, earthquake determined from strong ground motions*. Washington, DC: USGS.

Wentworth, C. M., and R. F. Yerkes. 1971. *Geologic setting and activity of faults in the San Fernando area, California*. Washington, DC: USGS.

Whittle, A. J., C. P. Aubeny, A. Rafalovich, C. C. Ladd, and M. M. Baligh. 1989. *Interpretation of in situ testing of cohesive soils using rational methods*. Washington, DC: Air Force Office of Scientific Research.

Wotherspoon, L., R. Orense, R. Green, B. A. Bradley, B. Cox, and C. Wood. 2013. "Analysis of liquefaction characteristics at Christchurch strong motion stations." In *Proc., New Zealand–Japan Workshop on Soil Liquefaction during Recent Large-Scale Earthquakes*. London: Taylor & Francis.

Yoshimine, M., H. Nishizaki, K. Amano, and Y. Hosono. 2006. "Flow deformation of liquefied sand under constant shear load and its application to analysis of flow slide in infinite slope." *Soil Dyn. Earthquake Eng.* 26 (2–4): 253–264. https://doi.org/10.1016/j.soildyn.2005.02.016.

Zhang, G., P. K. Robertson, and R. W. I. Brachman. 2002. "Estimating liquefaction-induced ground settlements from CPT for level ground." *Can. Geotech. J.* 39 (5): 1168–1180. https://doi.org/10.1139/t02-047.

Zhang, G., P. K. Robertson, and R. W. I. Brachman. 2004. "Estimating liquefaction-induced lateral displacements using the standard penetration test or cone penetration test." *J. Geotech. Geoenviron. Eng.* 130 (8): 861–871. https://doi.org/10.1061/(ASCE)1090-0241(2004)130:8(861).

Ziotopoulou, K., and R. W. Boulanger. 2013a. "Calibration and implementation of a sand plasticity plane–strain model for earthquake engineering applications." *Soil Dyn. Earthquake Eng.* 53 (Oct): 268–280. https://doi.org/10.1016/j.soildyn.2013.07.009.

Ziotopoulou, K., and R. W. Boulanger. 2013b. "Numerical modeling issues in predicting post–liquefaction reconsolidation strains and settlements." In *Proc., 10th Int. Conf. on Urban Earthquake Engineering (CUEE)*, 469–475. Tokyo: Tokyo Institute of Technology.

Ziotopoulou, K., and R. W. Boulanger. 2016. "Plasticity modeling of liquefaction effects under sloping ground and irregular cyclic loading conditions." *Soil Dyn. Earthquake Eng.* 84 (May): 269–283. https://doi.org/10.1016/j.soildyn.2016.02.013.